Doctoral Dissertation

博士論文

# Antisense piRNA biogenesis in *Bombyx* germ cells

（カイコ生殖細胞における二種類の

アンチセンスpiRNA生合成機構）

A Dissertation Submitted for Degree of Doctor of Philosophy
December 2019

令和元年12月博士（理学）申請

Department of Biological Sciences,
Graduate School of Science,
The University of Tokyo

東京大学大学院理学系研究科生物科学専攻

Kazuhiro Sakakibara

榊原　和洋

## Contents

# Abstract

## Abstract

PIWI-interacting RNAs (piRNAs) are germline enriched small RNAs to regulate the expression of transposons. To recognize target mRNA of transposon, piRNAs need to be antisense. Here I focus on two of three pathways for antisense piRNA biogenesis, primary pathway and secondary amplification pathway named ping-pong cycle and uncovered molecular mechanism of these pathways using Bombyx ovary derived culture cell-line (BmN4). BmN4 is the only culture cell derived from germ cell expressing two PIWI proteins, Siwi and Ago3, which associate with antisense piRNA, sense piRNA respectively. In primary pathway, I revealed that Zucchini (Zuc), a mitochondrial endonuclease cleaves 3´ end of Siwi-piRNA intermediate to maturate piRNA. Cleavage position by Zuc is not strictly regulated with sequence of piRNA intermediate. Owing to protection of ~25nt of piRNA intermediate from 5´ end by Siwi, Zuc can only cleave downstream region to produce mature piRNA. In ping-pong cycle, I revealed that Vreteno (Vret), a Tudor protein is essential for Ago3 dependent antisense piRNA production. Vret anchors Ago3-piRISC and Apo-Siwi at cytoplasmic granules called nuage in sDMA modification dependent manner to enhance Ago3-piRISC cleavage. In addition, arrest of ping-pong cycle by Siwi knockdown induces accumulation of targeting form of Ago3 as phosphorylated Ago3. Sequence analyses of the target RNA elucidated Ago3-piRISCs produce a few Siwi-piRNA intermediate successively.

# Abbreviations

## Abbreviations

| Abbreviation | Full name |
|---|---|
| APS | Ammonium Peroxodisulfate |
| Ago3 | Argonaute3 |
| Aub | Aubergine |
| β-Tub | β-Tubulin |
| Bm | *Bombyx mori* |
| CLIP | Crosslinking and Immunoprecipitation |
| DNA | Deoxyribonucleic acid |
| Dm | *Drosophila melanogaster* |
| DTT | Dithiothreitol |
| EDC | 1-Ethyl-3-(3-dimethylaminopropyl) carbodiimide |
| EDTA | Ethylenediaminetetraacetic acid |
| Endo | Endogenous |
| FBS | Fetal bovine serum |
| GST | Glutathione S-transferase |
| IP | Immunoprecipitation |
| KD | Knockdown |
| KDa | Kilodaltone |
| Luc | Luciferase |
| miRNA | Micro RNA |
| Mm | *Mus musculus* |
| mRNA | Messenger RNA |
| MS | Mass Spectrometry |
| Nbr | Nibbler |
| n.i. | Non-immune immunoglobulin |
| NP40 | Nonyl phenoxypolyethoxylethanol |
| nt | Nucleotide |
| PCR | Polymerase chain reaction |
| PBS | Phosphor buffered saline |
| P-Ago3 | Phosphorylated Ago3 |
| piRISC | piRNA-induced silencing complex |

| | |
|---|---|
| piRNA | PIWI-interacting RNA |
| rasiRNA | repeat-associated small interfering RNA |
| RG | arginine-glycine |
| RNA | Ribonucleic acid |
| RNAi | RNA interference |
| RRM | RNA recognition motif |
| RT-qPCR | reverse transcription quantitative PCR |
| sDMA | symmetrical dimethyl arginine |
| SDS | Sodium dodecyl sulfate |
| siRNA | Small interfering RNA |
| TE | Transposable element |
| TEMED | Tetramethylethylenediamine |
| TM | Transmembrane |
| T-PBS | 0.1% Tween 20 in PBS |
| Trim | Trimmer |
| Tris-HCl | Tris(hydroxymethyl)aminomethane hydrochloride buffer |
| Vret | Vreteno |
| WT | Wildtype |
| ZnF-MYND | MYND family zinc-finger |
| Zuc | Zucchini |

# 1. Introduction

# 1. Introduction

## 1.1. piRNA & PIWI protein: Guardians of germline genome

Germline genomes should be strictly protected to safely provide genetic information to next generation. However eukaryotic genomes themselves harbor transposable elements (TEs), which threaten host genomes by their transposition. Animals defend their germline genomes against TEs with RNA-mediated gene silencing which PIWI-interacting RNAs (piRNAs) and PIWI proteins play essential roles for. piRNAs are 23-30 nt small RNAs enriched in germ cells to detect target TEs with their complementarity. PIWI proteins are germline specific Argonaute proteins, which play crucial roles for transposon silencing as partners of piRNAs. Since only a single gene deficiency involved in the piRNA-mediated defense system induces infertility of animal, piRNAs and PIWI proteins are understood as indispensable guardians of germline genome.

piRNAs were discovered as repeat-associated small interfering RNA (rasiRNA) in the early 2000's by sequencing analyses of *Drosophila* testes and embryo (Aravin et al., 2003). rasiRNAs are several nucleotides longer than microRNAs (miRNAs), another class of small RNA, and were found to map to a variety of transposons. Experiments including the immunopurification of gonadal PIWI proteins revealed that rasiRNAs interact specifically with PIWI proteins (Girard et al., 2006; Klenov et al., 2007; Saito et al., 2006). Since the discovery, rasiRNAs have been known as PIWI-interacting RNAs (piRNAs), and piRNA-PIWI protein effector complexes have been recognized as piRNA-induced silencing complexes (piRISCs) (Brennecke et al., 2007; Ghildiyal and Zamore, 2009; Malone and Hannon, 2009). After the discovery, many scientists were attracted in this research field and piRNAs have been shown to be present in many animals, ranging from sponges to hydras, planarians, nematodes, flies, frogs, fish, and mammals, including humans. These piRNAs have been sequenced and computationally analyzed (Batista et al., 2008; Grimson et al., 2008; Hirano et al., 2014; Houwing et al., 2007; Lau et al., 2006; Lim et al., 2014; Robine et al., 2009; Shibata et al., 2016; Wilczynska et al., 2009). These researches revealed piRNAs play essential roles for germline genome integrity in many animals with PIWI proteins.

### 1.2. piRNA biogenesis pathways

The high level of conservation of the piRNA pathway across various species has enabled us to decipher the underlying molecular mechanisms by genetics and biochemical means using experimental model such as *Drosophila*. The current model of the piRNA pathway, focusing on piRNA biogenesis in *Drosophila* germ cells, is shown in Figure1. *Drosophila* has three hierarchal pathways, primary pathway, ping-pong cycle, phasing pathway as described below.

The primary pathway starts with transcription of the piRNA clusters in the genome, the primary origin of piRNAs, which contain many transposon remnants (Brennecke et al., 2007; Malone et al., 2009; Vagin et al., 2006). The transcripts, which are antisense against transposon mRNAs derived from the clusters, are processed through the primary biogenesis pathway, resulting in mature antisense piRNAs. Primary piRNAs are loaded onto two of three PIWI members Piwi and Aubergine (Aub) to form piRISCs. While Aub remains to be cytoplasmic upon becoming piRISC, Piwi is translocated to the nucleus and represses transposons at the transcriptional level.

Subsequently, primary piRNAs in germline cells are amplified through a feed-forward RNA cleavage cycle, known as the ping-pong cycle, by two PIWI endonucleases, Aub and Ago3, the third and last PIWI member in *Drosophila*. This secondary piRNA processing is cytoplasmic and consumes large amounts of RNA transcripts of transposons (and of piRNA clusters) as piRNA substrates, thus post-transcriptionally silencing transposons (Brennecke et al., 2007; Gunawardane et al., 2007; Li et al., 2009; Malone et al., 2009). Aub-bound piRNAs are rich in uracil at its 5´ end (1U) and are mostly antisense to transposon mRNAs, while Ago3-bound piRNAs show 10A bias and are oriented parallel to transposon mRNAs. This is because Ago3-bound piRNAs mainly originate from transposon mRNAs processed by Aub endonuclease activity in the ping-pong loop. These unique characteristics of piRNAs, often referred to as ping-pong signatures, are observed in many animals, indicating that the machinery is highly conserved.

A subset of piRNAs show ‘phasing’ similar to small interfering RNA (siRNA) (Han et al., 2015; Mohn et al., 2015). siRNA derives from a long double-stranded RNA precursor following cleavage by Dicer RNase III; however, phased piRNAs are produced in Dicer independent manner. Triggered by Ago3 cleavage, phased piRNAs are yielded from downstream region tandemly and loaded onto Piwi and Aub. Phased piRNAs are observed in other species, suggesting that it is a general feature of piRNA biogenesis.

### 1.3. Nuage and mitochondrion: piRNA biogenesis sites

piRNA factors, proteins involved in piRNA pathways, tend to be accumulated at the specific sites in cell. Two major sites are nuage and mitochondrion (Fig.2). Nuage is an electron-dense, non-membranous perinuclear granule (al-Mukhtar and Webb, 1971; Eddy, 1975). Nuage can be detected in nurse cells but is absent from the transcriptionally silent oocyte; thus, the presence of nuage seems to correlate with active transcription. Many piRNA factors including PIWI proteins, helicases and tudor-containing proteins are localized at nuage. Depletion of piRNA factors involved in ping-pong cycle tends to collapse the structure of nuage (Lim and Kai, 2007; Sato et al., 2015), suggesting that ping-pong cycle is closely related to nuage. Some piRNA factors including nucleases localize at mitochondrion and it is reported that these factors play roles for piRNA maturation (Izumi et al., 2016; Nishida et al., 2018). Nuage seems to be where piRISCs cleave longer RNAs such as transposon mRNAs or piRNA precursors and mitochondrion seem to be where nucleases cleave shorter RNAs, piRNA intermediates, to produce mature piRNAs. It is very interesting that different processing phases are held at different organelles but the reasons such organelles are selected are still in mystery.

## 1.4. BmN4: useful tool for piRNA biogenesis researches

Genetic screening using *Drosophila* uncovered many factors were involved in piRNA biogenesis (Czech et al., 2013; Handler et al., 2013) and expected that the molecular mechanism of piRNA biogenesis was complicated. Cultured cells are very useful tool for biochemical assays but cultured germ cells in *Drosophila* are not available unfortunately. Since BmN4 derived from *Bombyx mori* ovary is the only cultured germ cell already established, many researchers began to use BmN4 for piRNA biogenesis researches (Sakakibara and Siomi, 2018).

The *Bombyx* genome contains two piwi genes, *siwi* and *ago3* (Kawaoka et al., 2008b, 2008a), and are both expressed in BmN4 cells. *Bombyx* has only two biogenesis pathways, primay pathway and ping-pong cycle, and does not have the counterpart of *Drosophila* Piwi (Fig.3). *Bombyx* piRNA biogenesis pathway starts from association of Siwi and antisense piRNA intermediate. Upon Siwi-piRISC maturation, Siwi-piRISC cleaves mRNA of transposon. Cleaved sense-strand RNA is loaded onto Ago3 to be mature Ago3-piRNA (Nishida et al., 2015; Xiol et al., 2014). Ago3-piRISC cleaves antisense TE transcript and Siwi-piRNA is produced again (Fig.3). By comparing deduced amino acid sequences with those of Drosophila piRNA factors, silkworm piRNA genes have been readily determined. Some genes have already been experimentally shown to be necessary for piRNA biogenesis in BmN4 cells, mainly based on the results of RNAi-based knockdown experiments. BmN4 cells are simple to culture and easy to obtain large amounts of cell lysate to perform biochemical experiments, an advantage of the cell culture. Moreover, they are sensitive to RNA interference (RNAi), and proteins can be exogenously expressed via cDNA transfection. Therefore, BmN4 cells should be useful to decipher the mechanism of the ping-pong cycle, as well as its upstream primary biogenesis. Next four chapters explain important previous studies using BmN4 related to piRNA biogenesis.

### 1.5 Structure of Siwi-piRISC

piRNA maturation is not enough and piRISC formation is necessary to silence transposons. Thus many researchers tried to elucidate crystal structure of piRISCs however it had been mystery for a long time due to difficulty of purification of piRISCs. Finally, the crystal structure of endogenous Siwi-piRISC was determined a few years ago with unique strategy (Matsumoto et al., 2016). The complex was immunoisolated from BmN4 cells using anti-Siwi monoclonal antibodies, then treated with a tiny amount of thermolysine protease. This limited proteolysis digested the N-terminus of Siwi, which was assumed to be highly disordered based on previous structural studies of AGO-RISC. A large portion of C-terminal Siwi peptide, still bound with piRNA, was then released into the supernatant from the affinity resins.

The crystal structure showed that Siwi-piRISC consists of four domains, N, PAZ, MID, and PIWI, together with three linkers, L0, L1, and L2 (Fig.4A). MID domain holds $Mg^{2+}$ and 5´end of piRNA is captured in the pocket dependent on plus charge of $Mg^{2+}$. PAZ domain associates with 3´end of piRNA tightly interacting with 2´-*O*-methyl modification at the 3´end of piRNA. piRNA within piRISC is normally longer (~23-30 nt in silkworms) than guide RNA in AGO-RISC (~20-22 nt in most organisms). A comparison of peptide sequences shows that the PAZ domain in PIWI proteins has an additional stretch of amino acids that is absent in AGO members. In the Siwi-piRISC crystal structure, this stretch forms a protrusion at the inside of the piRNA 3´ end binding pocket (Fig.4B), which is absent from hAgo2-RISC. This may confer Siwi to accommodate piRNA, which is normally longer than guide RNA in AGO-RISC.

### 1.6. Papi: a mitochondrial tudor protein being scaffold for primary piRNA biogenesis

PIWI proteins typically possess symmetrically dimethylated arginines (sDMAs) in arginine-glycine (RG) repeat(s) that are mostly located at the N-terminal region (Kirino et al., 2009; Liu et al., 2011; Nishida et al., 2009; Vagin et al., 2009). The responsible factor of the post-translational modification is Capsuleen/PRMT5/DART5 (Kirino et al., 2009; Nishida et al., 2009; Vagin et al., 2009). Earlier literatures showed that most, if not all, of sDMAs in PIWI proteins associate with the Tudor domain of specific Tudor domain-containing proteins (Siomi et al., 2010). Papi is one of the most focused Tudor domain-containing proteins in piRNA field, which also have transmembrane (TM) region and two KH domains (Honda et al., 2013). The KH domain is a RNA-binding domain found in a wide range of proteins playing key roles in RNA metabolism.

Recent studies revealed that Papi is an essential primary piRNA biogenesis factor to assemble Siwi and piRNA intermediates hierarchically (Nishida et al., 2018). Firstly, Apo-Siwi associates with Papi in sDMA dependent manner. Secondary, Siwi-piRNA intermediate is loaded onto Siwi anchored by Papi. Thirdly, 3´ sides of piRNA intermediates are stabilized by interaction with KH domains of Papi (Fig.5). 9RK mutant of Siwi, which abolish sDMA modification sites, completely lost the interaction with Papi and piRNA intermediates and the mutant is not able to be piRISC form in result. KH mutant of Papi does not have abilities to bind RNA and play a role for piRNA biogenesis. Papi-Siwi interaction allows the 5′ end of the piRNA intermediate to locate within the piRNA 5´ binding pocket of Siwi in MID domain. Papi-piRNA intermediate interaction through maintains 3´ end stability of piRNA intermediates as alternative to PAZ domain in mature piRISC case (see section 1.5).

### 1.7. Trimmer, Nibbler, Zucchini: Nucleases playing roles for piRNA biogenesis

Trimmer (Trim) is an exonuclease composed of CAF1 family ribonuclease and TM domains, which is localized on the surface of mitochondrion as Papi. Trim was identified by mass spectrometric analysis of protein components within the Papi complex (Izumi et al., 2016). In vitro experiments showed that Trim had the activity to remove extra nucleotides from the 3´ end of RNAs of 50 nt long that has been pre-loaded onto Siwi to the piRNA size (i.e., ~27-nt long). Thus Trim seems to be a trimming factor for 3´ end of piRNA.

Nibbler (Nbr) is also an exonuclease consisting of RNaseH-like and Mut7-C RNase domains. Nbr is originally identified in *Drosophila* in trimming the 3´ end during miRNA maturation. Recent study revealed that not only miRNA but also piRNA are affected by *nbr* mutation in *Drosophila* (Hayashi et al., 2016). Since, aberrant long piRNAs, whose 3´ ends are extended, were observed in *nbr* mutant fly, Nbr is also considered as 3´ trimming factor of piRNAs.

Zucchini (Zuc) is an endonuclease, which specifically cleave single strand RNAs and anchored on the mitochondrial outer membrane through TM domain like Papi (Ipsaro et al., 2012; Nishimasu et al., 2012). Zuc has been well-studied with germline somatic cell in *Drosophila* playing an essential role for somatic primary piRNA maturation. All these three nucleases are expressed in BmN4 but how they work for piRNA production in BmN4 was not clear (Fig.6).

### 1.8. Vasa: a helicase driving first half of ping-pong cycle

While large part of ping-pong cycle had not been clearly understood, first half of ping-pong cycle has already bean studied. BmN4 largely contributed to uncover the molecular mechanism of first half of ping-pong cycle.

PIWI-piRISC retains its cleavage products on the complex even after target RNA cleavage (Nishida et al., 2015). However, the ping-pong pathway would be disturbed if piRISC retains the cleaved RNAs long-term. Therefore, a co-factor is required to release cleaved RNAs from piRISC only when new piRNAs can be produced: namely, when piRNA-free Ago3 associates with the Siwi-piRISC-cleaved RNA complex in the case of BmN4 cells. DEAD-box RNA helicase was determined to be such a co-factor in the release of cleaved RNAs from Siwi-piRISC (Nishida et al., 2015; Xiol et al., 2014). This reaction requires the RNA helicase and ATP hydrolysis activities of Vasa protein (Fig.7). Vasa associates with Siwi-piRISC, but not with Ago3-piRISC. In vitro assays showed that Vasa displaced cleaved RNA from Siwi-piRISC, but not from Ago3-piRISC. These observations suggest that Vasa specifically drives first half of ping-pong cycle with its helicase activity.

### 1.9. Aim of this study

The main goal of this study was to elucidate the molecular mechanism of two different antisense piRNA pathways, primary pathway and ping-pong cycle. Previously, screenings for piRNA factors were performed and many genes were identified (Czech et al., 2013; Handler et al., 2013). In addition, phenotypic defects by depletion of such genes were widely observed using mutant animals. Expression changes of piRNAs were also analyzed by piRNA-seq using mutant animals. However, molecular mechanism underlying such defects and molecular function of piRNA factors were not clearly understood. Since insufficiency of biochemical experiment on piRNA factors is critical reason of unclear molecular mechanism, I selected BmN4 cell, the only cultured cell derived from germ cell, as experimental tool and tried to uncover the molecular mechanism of piRNA biogenesis by biochemical assays. Primary pathway and ping-pong cycle were focused on because they are only biogenesis pathways existing in BmN4.

First question is what the indispensable nuclease for primary piRNA maturation is. Previous studies identified three nucleases, Zuc, Trim and Nbr, as piRNA factors but they mainly relied on in vitro assays and sequence analyses. How they play roles for piRNA biogenesis was not clearly mentioned. Therefore, my first project is the identification of responsible nuclease for primary piRNA and elucidation of the function of the nuclease with biochemical assays. Second question is how Ago3-piRISC produce Siwi-piRNA. Second half of ping-pong cycle is especially not clearly understood. Major reason is that depletion of the factors working at this phase does not change the amount of Siwi-piRNA owing to compensation by primary pathway. In other words, there are not good strategies to evaluate second half of ping-pong cycle. My second project is that elucidation of molecular mechanism of Ago3-dependent piRNA biogenesis overcoming such difficulties. Finally I aimed comprehensive understanding of antisense piRNA production in *Bombyx* germ cell.

### 1.10. Summary of this research

This study uncovers molecular mechanism of two different antisense piRNA biogenesis pathways in BmN4 cells. In primary pathway part, knockdown assays showed knockdown of Zuc reduced the amount of Siwi-piRNA and induced accumulation of Siwi-piRNA intermediates in Papi complex whereas knockdown of Trim or Nbr does not. Papi immunoprecipitation from mitochondrial fraction revealed Zuc were involved in Papi complex together with Siwi. These data strongly suggests Zuc cleaves piRNA intermediates to produce mature piRNA within Papi complex on mitochondria. *In vitro* reconstruction assays with recombinant GST-Zuc, Flag-Siwi and $^{32}$P-labeled synthetic RNAs revealed that Zuc cleaved 3´ ends of RNAs avoiding ~25nt from 5´ ends protected by Siwi. *In vitro* cleavage assay showed Zuc cleaves RNAs without strong nucleotide bias. The *in vitro* assays suggest that cleavage site of Zuc is mainly determined by Siwi and Zuc plays a role just as scissors.

In ping-pong cycle part, I focused on the functions of Vret because it was a strong interactor of Ago3. Firstly Ago3 dependent Siwi-piRNAs were identified from sequence to design probes for northern blotting assays to detect the change of amount of Siwi-piRNAs derived from ping-pong cycle. Northern blotting with such probes revealed that knockdown of Vret reduced Ago3 dependent Siwi-piRNAs whereas the amount Ago3-piRISC did not change. Interestingly, Vret associated with Ago3-piRISC and Apo-Siwi selectively. Both of them could not localize at nuage without Vret. Knockdown of Vret also induced the defect of Ago3 cleavage. According to the experiments, I concluded Vret is scaffold protein anchoring Ago3-piRISC and Apo-Siwi at nuage to enhance Ago3's target cleavage for Siwi-piRNA production. Furthermore I arrested ping-pong cycle by Siwi depletion to research target-binding Ago3-piRISCs and found Ago3s were aggregated at nuage and phosphorylated in Siwi-depleted condition. Immunoisolation of phosphorylated Ago3s (P-Ago3s) revealed P-Ago3s held two different lengths of target RNAs. Sequence analyses of the RNAs showed longer RNAs were to be Siwi-piRNA intermediates and shorter RNAs were byproduct. Further analyses reveals Ago3s produced Siwi-piRNA intermediates tandemly. I also made progress in how Ago3-piRISCs produce Siwi-piRNA intermediates as above.

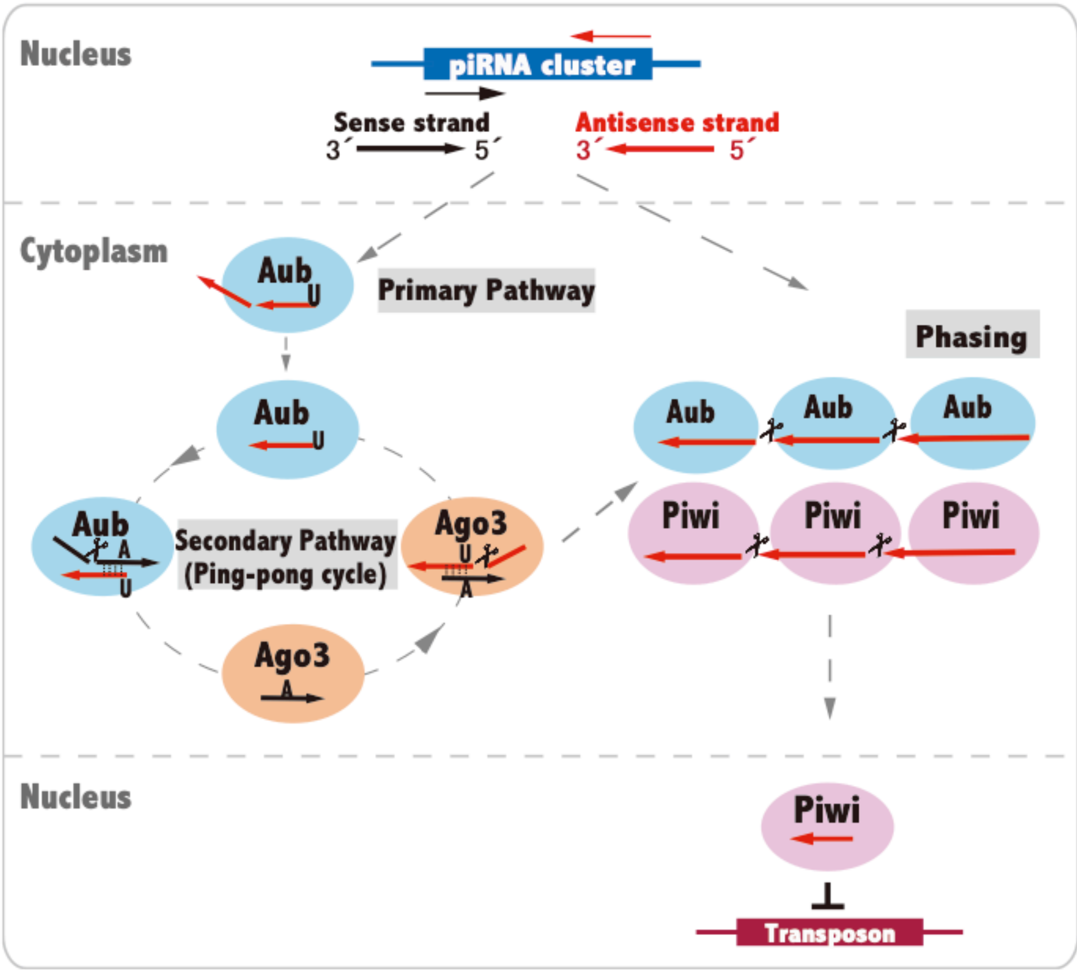


**Fig. 1. piRNA biogenesis model in *Drosophila* germ cell**

*Drosophila* has three biogenesis pathways, primary pathway, ping-pong cycle and phasing.

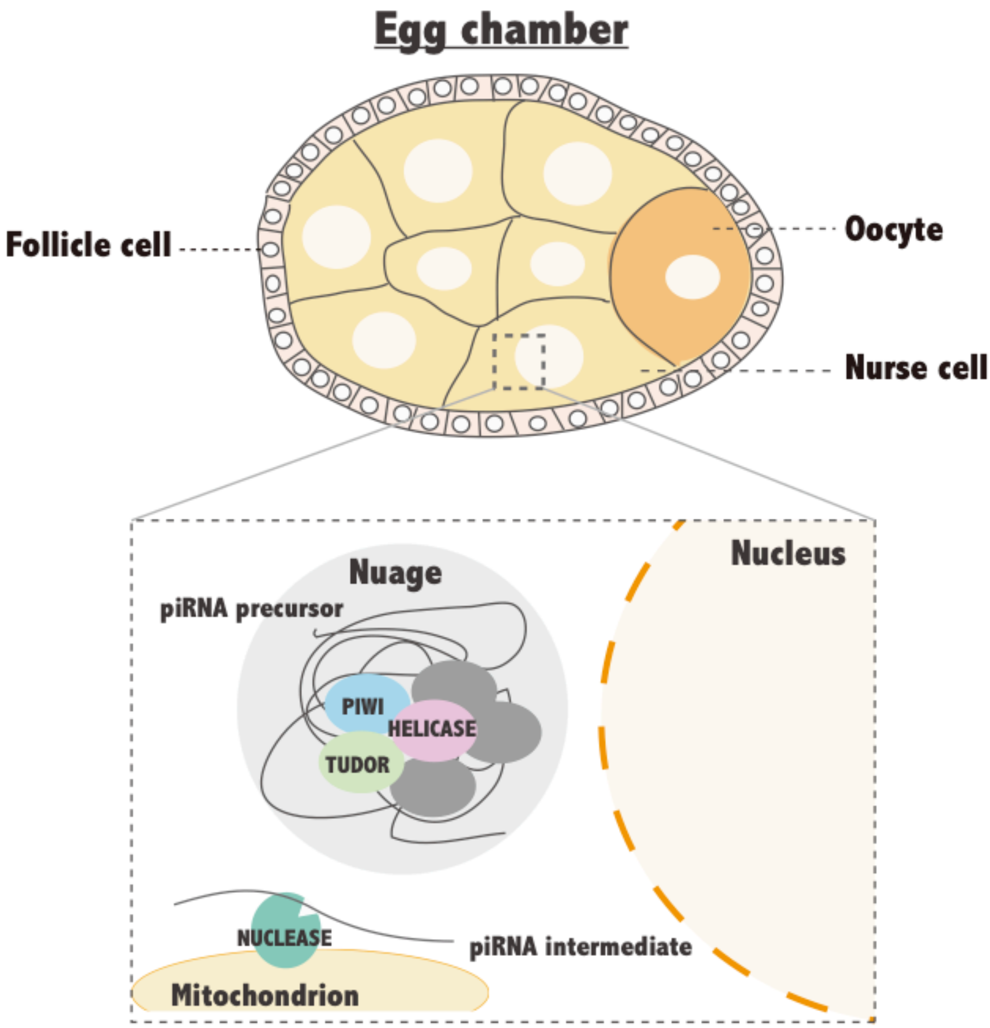


**Fig. 2. Structure of egg chamber and piRNA biogenesis sites in nurse cell**

Egg chamber is composed of follicle cell, nurse cell and oocyte. Follicle cell is germline somatic cell localized at outer layer of egg chamber, which has simpler piRNA biogenesis pathway with one PIWI protein. Nurse cell and oocyte are germ cell but nurse cell only has active piRNA system. Nuage and mitochondrion in nurse cell are important sites for piRNA biogenesis.

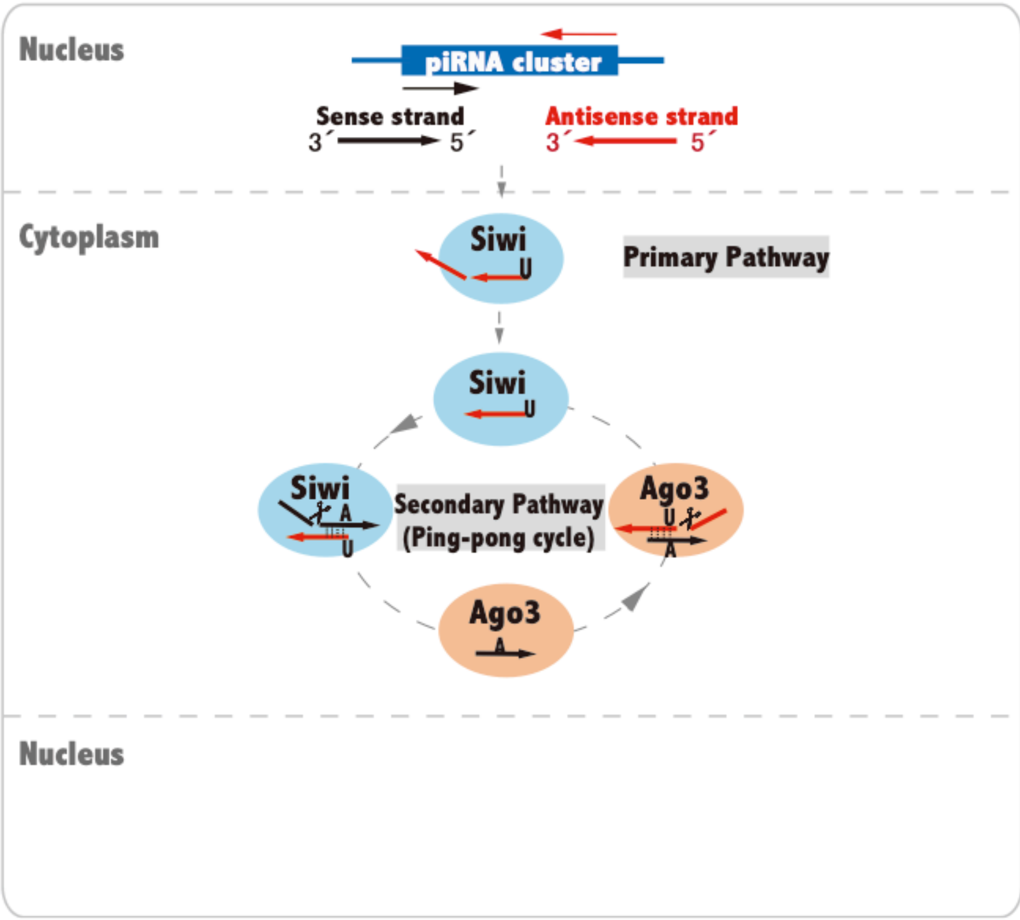


**Fig. 3. piRNA biogenesis model in *Bombyx* germ cell**

*Bombyx mori* express only two PIWI proteins, Siwi and Ago3, lacking nuclear PIWI protein as Piwi in *Drosophila*. Primary pathway and ping-pong cycle exist in *Bombyx* and Siwi-piRNAs are produced in both pathways.

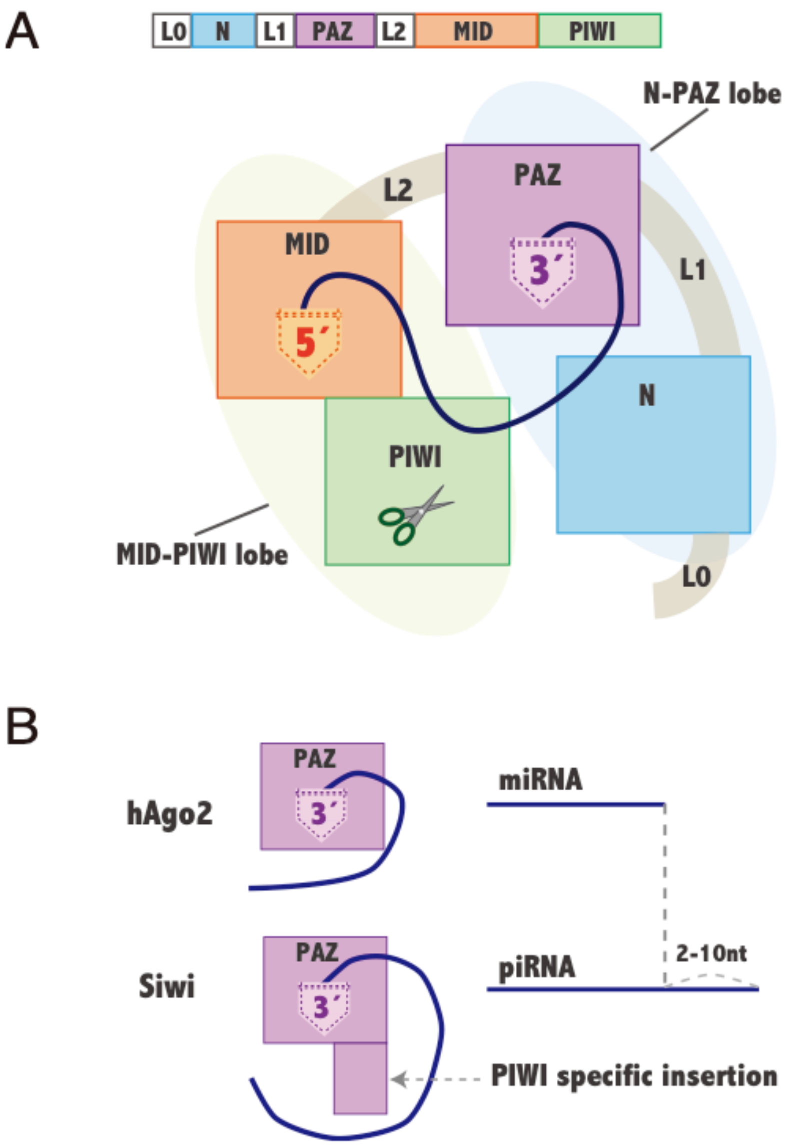


**Fig. 4. Structure of Siwi-piRISC**

(A) Siwi is composed of 4 domains and 3 linker regions and can be divided into two lobes (N-PAZ and MID-PIWI). MID domain has 5´ binding pocket of piRNA and PAZ domain has 3´ binding pocket. PIWI domain has piRNA-dependent endonuclease activity to repress transposons. (B) Structural difference in PAZ domain between hAgo2 and Siwi reflecting difference in length between miRNA and piRNA.

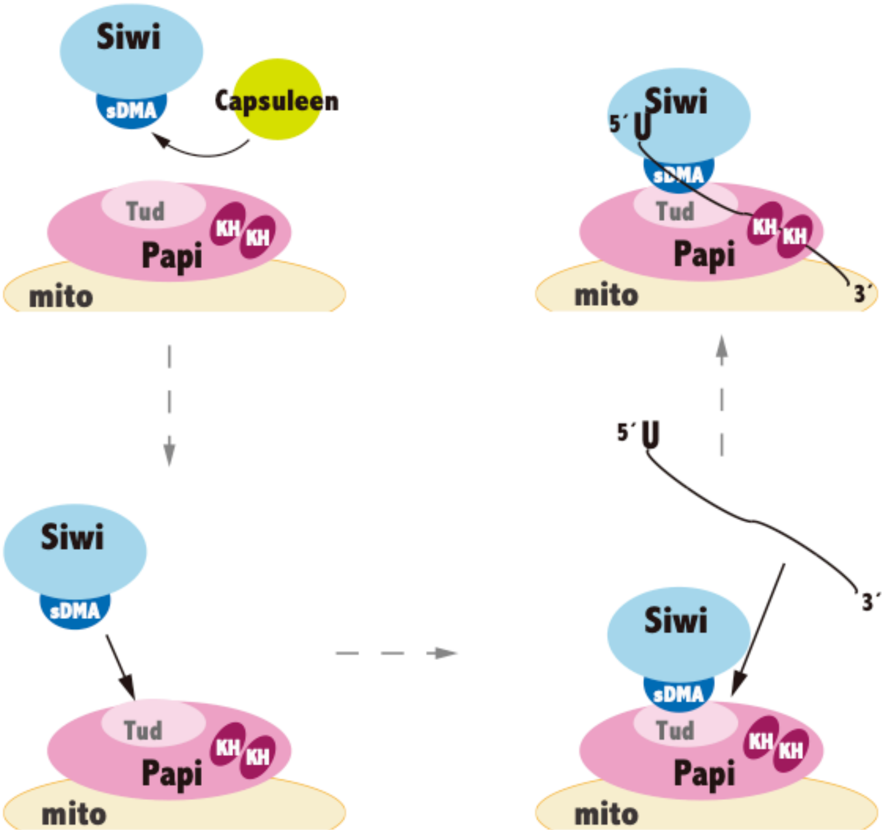


**Fig. 5. Key factors for primary pathway in *Bombyx* are accumulated on Papi hierarchically.**

After Capsuleen adds sDMA modification to Siwi, Siwi associate with Papi dependent on the modification. Upon this, 5´ end of piRNA intermediate is loaded onto Siwi. 3´ end region of piRNA intermediate is stabilized by KH domains of Papi.

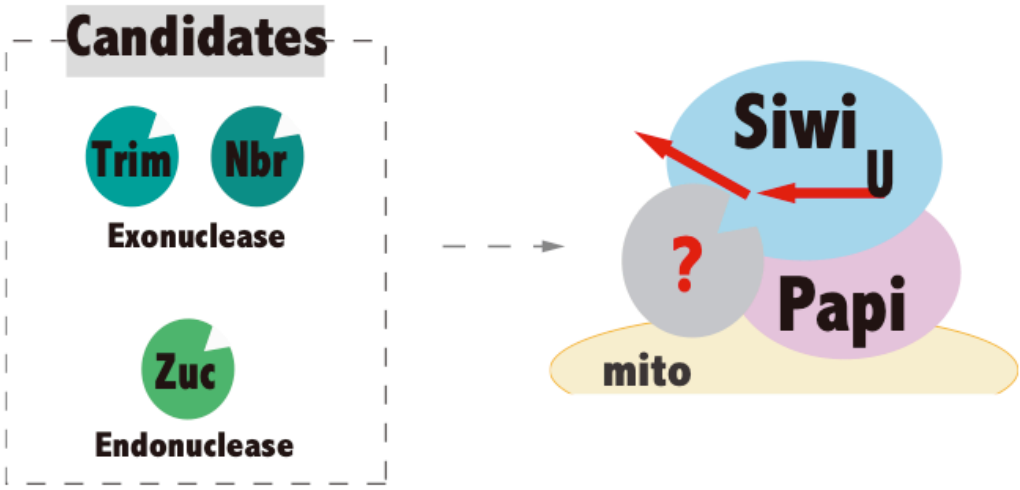


**Fig. 6. Working hypothesis of primary piRNA maturation**

Previous researches on Papi raised possibility that piRNA maturation was performed in Papi-Siwi complex. According to the researches, responsible nucleases for piRNA maturation were pared down to three genes; *trim*, *nbr* and *zuc*.

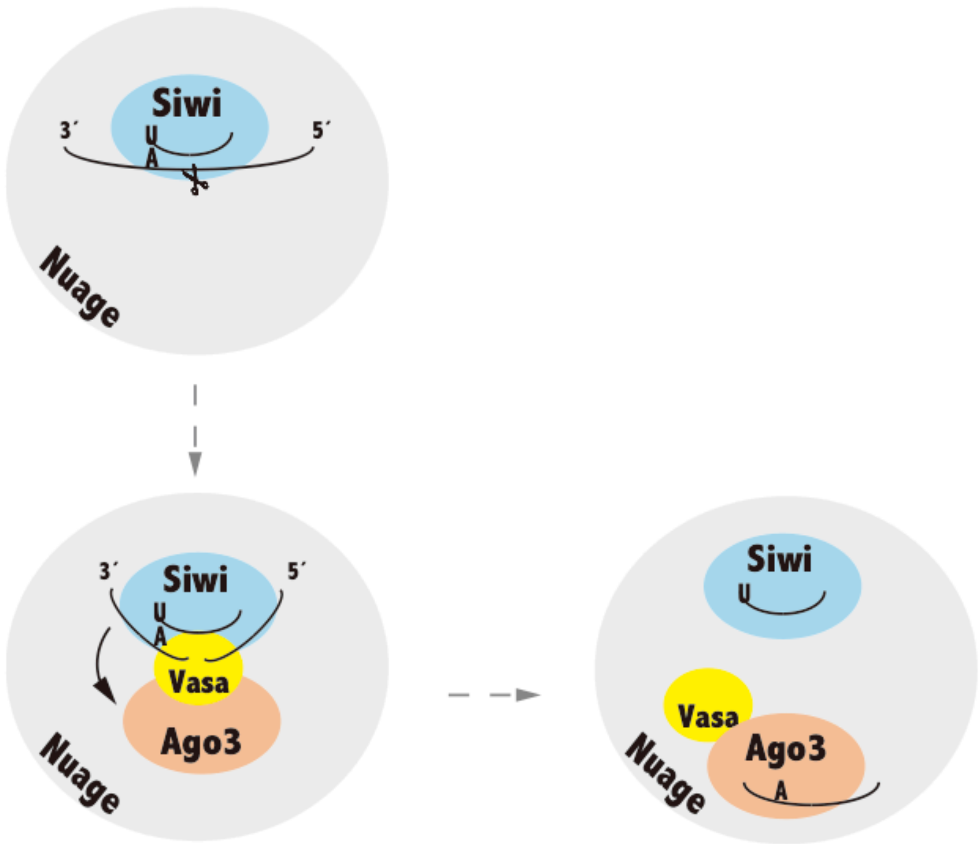


**Fig. 7. Vasa releases cleavage products from Siwi and loads them onto Ago3**

Siwi-piRISC cleaves mRNA of transposon and holds tightly. Vasa, a DEAD-box RNA helicase, release cleavage products in ATP dependent manner. Cleavage product is loaded onto Ago3 to be Ago3-piRISC.

# 2. Material and methods

## 2. Material and methods

### 2.1. Cell culture

BmN4 cells are cultured in EX-CELL(TM) 420 Serum-Free Medium for Insect Cells (SAFC Biosciences) with 10% FBS (Equitech-Bio) and Penicillin-Streptomycin-Glutamine (100X) (Thermo Fisher Scientific). Cell medium is changed in every 3 days.

### 2.2. RNAi and transgene expression

BmN4 cells ($1 \times 10^6$cells) were transfected with 500 pmol of siRNA duplex in 100 μl of EP buffer (137mM NaCl, 5mM KCl, 0.5mM $Na_2HPO_4$, 2.1mM HEPES-KOH (pH7.1)). Transfection was conducted in electroporation cuvettes using a Nucleofector device (Amaxa Biosystems). Upon transfection, cells were incubated at 27°C for 72 hr. siRNA transfection was performed again to ensure the RNAi effect. The sequences of the siRNAs are summarized in Table1. Luc siRNA was used as a control. To express proteins in BmN4 cells exogenously, the cells ($6 \times 10^5$cells) were transfected with 2 μg of plasmid in 5 μl of FuGENE HD transfection reagent. After transfection, cells were incubated at 27°C for 48 hr.

### 2.3. Plasmid construction

pIB-myc and pIB-3xFlag were generated using a pIB vector (Thermo Fisher Scientific). Vectors to express Flag-Vret-L/S were generated by inserting Vret-L/S cDNAs into pIB-3xFlag, respectively. Plasmid expressing mutants of Flag-Siwi, Ago3, Vret were generated by inverse PCR. The PCR primers used are summarized in Table 1.

### 2.4. Northern blotting

Total RNAs were isolated from 4 × $10^5$ BmN4 cells using ISOGENII (NIPPON GENE) according to manufacturer's instructions. 5μg of total RNAs were resolved by electrophoresis. RNAs are transferred to neutral nylon membrane, Hybond-N (GE Healthcare), and fixed with EDC cross-linking solution as previously described (Pall and Hamilton, 2008). After pre-hybridization with hybridization buffer (200mM Sodium phosphate (pH 7.2), 7% SDS, 1mM EDTA), hybridization was performed with 100pM DNA probe in hybridization buffer for 15hr at 42°C. Membrane is washed with 2×SSC buffer (30mM Sodium citrate, 300mM NaCl, 0.1% SDS) three times. Upon exposure to imaging plate, images are obtained by Typhoon FLA 9500 (GE Healthcare). Sequences of the probe DNA are shown in Table 1.

### 2.5. Western blotting

Samples for western blotting are diluted with 2×sample buffer (0.125M Tris-HCl (pH 6.8), 4% SDS, 19% Glycerol, 0.2M DTT, 0.01% BPB). Upon electrophoresis, proteins are transferred to nitrocellulose or PVDF membranes (Wako). After blocking with 5% skim milk for 30min, 1ng/μl antibodies in 0.1% Tween containing PBS (T-PBS) are mounted on membranes for 1hr at room temperature. Membranes are washed three times with T-PBS and 1ng/μl Anti Mouse IgG (H+L) HRP (MP Biomedicals) in T-PBS are mounted on membranes for 1hr at room temperature. Membranes are washed five times with

T-PBS and images are obtained by ChemiDoc (Bio-Rad) with Clarity ECL substrate (Bio-Rad)

### 2.6. Immunoprecipitation from BmN4

15µl of Dynabeads (Thermo Fisher Scientific) and 1.5µg of antibodies were incubated in 500µl of 0.02% Tween-PBS (T-PBS). $6\times10^5$ cells of BmN4 were lysed with immunoprecipitation(IP) buffer (30 mM HEPES-KOH (pH 7.3), 150 mM KOAc, 2 mM MgOAc, 5 mM DTT, 0.1% NP-40, 2 µg/mL Pepstatin, 2 µg/mL Leupeptin, and 0.5% Aprotinin). After centrifugation, the lysate was mixed with antibodies-conjugated dynabeads at 4°C for 1 hour (For Papi-IP, 0.5% Triton-X was used instead of 0.1% NP-40. For phosphorylated Ago3 (P-Ago3)-IP, 1% Empigen was used instead of 0.1% NP-40.). After immunoprecipitation, the beads were washed extensively with IP buffer.

### 2.7. Sucrose density gradient centrifugation

Mitochondria were prepared as described previously (Wieckowski et al., 2009). The mitochondrial pellet was resuspended in gradient buffer (30 mM HEPES (pH 7.4), 100 mM potassium acetate, 1 mM DTT, 4 mM magnesium acetate, and 1% Tergitol-type NP-40), and centrifuged at 14,000*g* at 4 °C for 30 min. The supernatant was placed at the top of a 10–40% sucrose gradient and centrifuged in a Beckman MLS-50 rotor at 178,000*g* at 4 °C for 16.5 hr.

### 2.8. Recombinant protein preparation

The cDNA encoding Zuc excluding MLS (residues 29–206) was cloned into pCold-GST vector. The Zuc mutant (H141A) was generated from pCold-Zuc by inverse PCR. The protein was purified using glutathione-Sepharose (GE Healthcare) with purification buffer (20 mM Tris-HCl (pH 8.0), 150 mM sodium chloride and 1 mM DTT). The proteins were treated with HRV3C protease (GE Healthcare) to remove the GST tag and further purified by Enrich S (Bio-Rad). To yield pIZ-3xFlag-Siwi, 3xFlag-Siwi was amplified from pIB-3xFlag-Siwi (Nishida et al., 2015) by PCR and inserted into pIZ vector (Thermo Fisher). Flag–Siwi was immunoisolated by ANTI-FLAG M2 Affinity Gel (Sigma) from BmN4 cells and eluted by 500 ng/µl 3× Flag peptide (Sigma).

## 2.9. *In vitro* processing assay

The synthesized RNAs (GeneDesign) were $^{32}P$-labelled at their 5´ end. The sequences of RNAs are indicated in Table 1. Radiolabelled int-piRNAs ($10^4$ c.p.m.) were incubated with 0.1 µg of recombinant Zuc in 20 µl of buffer A (Nishimasu et al., 2012) at 26 °C for 30 min. A total of 1 µl of 1 µM radiolabelled int-piRNAs and 200 ng of purified Flag-Siwi were mixed at 26 °C for 30 min in 20 µl of the loading buffer (30 mM HEPES (pH 7.4), 100 mM potassium acetate, 2 mM magnesium acetate, 20 mM creatine monophosphate, 1 mM ATP, 0.15 U/µl creatine phosphokinase, 1 mM DTT and 0.5 U/µl RNasin (Promega)). After loading, the Flag-Siwi-containing mixture was incubated with Dynabeads (with anti-Siwi antibody or Papi immunoprecipitation product) at 4 °C for 1 hr. The beads were then washed five times with binding buffer. RNAs were isolated from the beads with phenol-chloroform and precipitated with ethanol. They were then resolved by denaturing PAGE. Immunopurified Papi complexes were incubated with 1 µg of recombinant Zuc in 30 µl of buffer A containing 2.5 mM EGTA and 0.1 U/µl RNasin at 27 °C for 0-180 min. RNAs were isolated from the beads with phenol-chloroform and precipitated with ethanol, after which they were transferred to Hybond-N (GE Healthcare). Following protocol is the same as 2.4.

### 2.10. Cloning of Vret

Vret cDNAs corresponding to the particular regions were obtained by RT-PCR using total RNAs from BmN4 cells. Vret-L and -S were identified by 5´ race with SMARTer® RACE 5´/3´ Kit (Clontech). The PCR primers are summarized in the Table1.

### 2.11. Production of monoclonal antibody

Mouse was immunized with bacterially produced glutathione S-transferase (GST)-tagged Vret-L (amino acids 466-669). To produce GST-Vret, Vret is cloned into pGEX5X vector. The GST-tagged protein was expressed in BL21 (DE3) and purified using glutathione-Sepharose (GE Healthcare) with purification buffer (20 mM Tris-HCl (pH 8.0), 150 mM sodium chloride and 1 mM DTT).

### 2.12. CLIP

CLIP was performed as described previously (Jaskiewicz et al., 2012). Dephosphorylation and RNA radiolabelling with $^{32}P$ were performed using T4 polynucleotide kinase (NEB).

### 2.13. Dephosphorylation treatment

Immunopurified Ago3 was incubated with Antarctic Phosphatase (NEB) at 37°C for 30min for dephosphorylation.

### 2.14. Sample preparation for Mass Spectrometry (MS)

Trypsin digestion was performed using a robot (ProGest, DigiLab) with the following protocol: Washed with 25mM ammonium bicarbonate followed by acetonitrile. Reduced with 10mM DTT at 60°C followed by alkylation with 50mM iodoacetamide at RT. Digested with trypsin (Promega) at 37°C for 4hr. Quenched with formic acid and supernatant was analyzed directly without further processing.

### 2.15. Mass Spectrometry

The gel digest was analyzed by nano LC/MS/MS with a Waters NanoAcquity HPLC system interfaced to a ThermoFisher Q Exactive. Peptides were loaded on a trapping column and eluted over 75µm analytical column at 350nl/min; both columns were packed with Luna C18 resin (Phenomenex). The mass spectrum was operated in data-dependent mode, with MS and MS/MS performed in the Orbitrap at 70,000FWHM resolution and 17,500 FWHM resolution, respectively. The fifteen most abundant ions were selected for MS/MS.

### 2.16. Data processing

Data were searched using a local copy of Mascot with the following parameters:

Enzyme: Trypsin. Database: Uniprot Bombyx mori (concatenated forward and reverse plus common contaminants). Fixed modification: Carbamidomethyl (C). Variable modifications: Oxidation (M), Acetyl (Protein N-term, K), Deamidation (NQ), Phospho (STY), GG (K), Methyl (K). Mass values: Monoisotopic. Peptide Mass Tolerance: 10ppm. Fragment Mass Tolerance: 0.02Da. Max Missed Cleavage: 2.

Mascot DAT files were parsed into the Scaffold software for validation, filtering and to create a nonredundant list per sample. Data were filtered using a minimum protein value of 90%, a minimum peptide value of 50% (Prophet scores) and requiring at least two unique peptides per protein. Scaffold results were exported as mzIdentML and imported into Scaffold PTM in order to assign site localization probabilities using A-Score (Beausoleil et al., 2006).

### 2.17. Immunofluorescence

BmN4 Cells are placed on 0.075% poly-L-lysine coated cover glass. Cells are fixed with 2% formaldehyde in PBS for 15min and permeabilized with 0.1% Triton X-100 in PBS for 15min. After blocking with 3% BSA in PBS for 15min, cells are covered with 1ng/µl 1$^{st}$ antibodies diluted with 3% BSA in PBS for 1hr. 2$^{nd}$ antibodies (Alexa 488/Alexa Fluor 555 goat anti-mouse immunoglobulin G 1 (IgG1)/IgG2a antibodies (Invitrogen)) in 3% BSA in PBS cover cells for 1hr at dark room. Cover glasses are mounted with VECTASHIELD® Antifade Mounting Medium with DAPI (VECTOR LABORATORIES). All steps are conducted at room temperature. Before every step, cells are washed with

PBS three times. When Flag-tag containing proteins or Siwi are stained, cells are treated with 35μg/ml digitonin in PBS for 5 min before fix. All images were collected using a Zeiss LSM710 laser-scanning microscope with C-Apochromat 40x/1.20 W Korr objective lens at room templature. Cells are illuminated with 30mW 405nm diode laser (laser power 5%, pinhole 2.82 airy unit), 25mW 488nm argon laser (laser power 10%, pinhole 0.82 airy unit) and 1.2 mW 543nm HeNe laser (laser power 2%, pinhole 2.18 airy unit). Pixel dwell time was set to be 6.3μs and 8 sequentially scanned images were averaged.

### 2.18. RNA isolation and generation of Ago3-associated RNA libraries

Ago3 and P-Ago3 were immunoisolated with IP buffer containing 500 mM sodium chloride. RNAs were isolated from the immunoprecipitates by phenol-chloroform and precipitated with ethanol. RNAs of 12-18, 23-35 and 50-100 nucleotides in length were eluted from the gels respectively as Target-S, piRNA and Target-L. RNA libraries were produced from the RNAs with NEBNext® Small RNA Library Prep Set for Illumina (NEB).

### 2.19. Analysis of Ago3-associated RNA sequences

Libraries were sequenced using Illumina MiSeq (single-end, 51 cycles). After adaptor sequences were removed from obtained reads, for Ago3-piRNAs, a total of 1,331,305 reads were obtained from control sample, 1,613,608 reads from Siwi-knockdown sample. For Ago3-associated target RNAs, a total of 2,155,565 reads were obtained from Target-S sample, 8,267,028 reads from Target-L sample. The reads were mapped to 121 *Bombyx mori* transposon consensus sequences (a gift from S. Kawaoka) using Bowtie2, allowing up to one mismatch for Target-L. For others, reads were mapped to the transposons using bowtie, allowing no mismatch. Using transposon-mapped reads, length distribution and strand bias were calculated. The reads were also mapped to the *Bombyx mori* reference genome (downloaded from Silkbase; silkbase.ab.a.u-tokyo.ac.jp) using bowtie2 and bowtie as above. Using genome mapped reads, ping-pong signatures were calculated and phasing analyses were conducted.

## Table1. Sequences of oligonucleotides

| Experiment | Name | Sequence |
|---|---|---|
| Plasmid Construction | Ago3-K637A-L | GCGAAAGTTTGTTGTGCTGACAA |
| | Ago3-K637A-R | AATGGCCGCGTATCTGTCGT |
| | Ago3-sires-L | GAGGTGTGGCCGGGTTATGTTACAGCAGTAGACGAATACGAAGG |
| | Ago3-sires-R | TAATTTATGCTGAGGTATCTGTATG |
| | Ago3-4SA-1-L | AAAGCAAGCGCTCAAGTAGCAAGCA |
| | Ago3-4SA-2-L | AGACAGCTTCAGTTGCCAAGAACAA |
| | Ago3-4SA-1-R | GTGCTGAAACTGCAGTTTCAGACATTT |
| | Ago3-8SA-1-L | AAAGCAGCCGCTCAAGTAGCAAGCAG |
| | Ago3-8SA-1-R | TTGAGCGGCTTGCAAGTTCTGAAGC |
| | Ago3-8SA-2-L | CAGACAGCTGCAGTTGCCAAGAACAAA |
| | Ago3-8SA-2-R | TGCTGCAACTGCAGTTTCAGCCATTTTTTC |
| | Vret-tudor1mut-L | GAAGCTGGCGCCATTGAAATAACTCAGCTG |
| | Vret-tudor1mut-R | AATAGCTTCAAGTAAATATTTGTTTTTGTT |
| | Vret-tudor2mut-L | GACGCCGGCGCCGTTGCCGAGGT |
| | Vret-tudor2mut-R | CACGGCCAGCACGCGCGCGGTG |
| | Vret-sires-L | AGCCTTTGACAACATTCTTCAAGATGTGCT |
| | Vret-sires-R | TTCTGCGAGCGCGTGTCGGC |
| | Vret-antigen-L | CGACGGACCCTCGTACCGGA |
| | Vret-antigen-R | GATCTCCGGACGAGGAACTT |
| | pCold-vector-L | AATTCAAGCTTGTCGACCTGCA |
| | pCold-vector-R | GGATCCCTCGAGGGTACCGA |
| | pCold-Zuc-L | TACCCTCGAGGGATCCAAGAAGAAGAAAGAA |
| | pCold-Zuc-R | CGACAAGCTTGAATTTTAACTGGTTATTGG |
| | Zuc-H141A-L | GCCCACAAGTTCTGCATAATAGATG |
| | Zuc-H141A-R | CATTAGATTTGTAGACTTCATCCAG |
| Northern blotting | RT3-1 | ACCAGCCGATCGTCATCGCATCCGTTTA |
| | RT3 | CCCAGCCGATCGTCATCGCATCCGTTTA |
| | R2Bm | GAGGTTGGAGATTTTGAGAGCTCATCTGA |
| | Bmmar6 | CGTCCAGATTTGAATCCGTTAGATTACA |
| | Pao | AAACAGCGAATCAGAATACAGTAAGTCA |
| RNA i | T7-dsLuc-L | TAATACGACTCACTATAGGGGGAGAGCAACTGCATAAGGC |
| | T7-dsLuc-R | TAATACGACTCACTATAGGGTCCCTATCGAAGGACTCTGG |
| | T7-dsZuc-L | TAATACGACTCACTATAGGGATGGCAGTAACTCTTAGTAA |
| | T7-dsZuc-R | TAATACGACTCACTATAGGGGTCCAGTTCAATGACCCTGC |
| | T7-dsTrim-L | TAATACGACTCACTATAGGGTTCAGAAGTTTCAAAATGGT |
| | T7-dsTrim-R | TAATACGACTCACTATAGGGAGCGAAGAATTCATACAAAT |
| | siLuc sense | *CGUACGCGGAAUACUUCGA*TT |
| | siLuc antisense | *UCGAAGUAUUCCGCGUACG*TT |
| | siSiwi sense | *CACUCGGAGGAUAUCUCUU*TT |
| | siSiwi antisense | *AAGAGAUAUCCUCCGAGUG*TT |
| | siAgo3 sense | *GUUUGGCCUGGAUACGUAA*TT |
| | siAgo3 antisense | *UUACGUAUCCAGGCCAAAC*TT |
| | siSpn-E sense | *CAGACACUCGUAUACAUUA*TT |
| | siSpn-E antisense | *UAAUGUAUACGAGUGUCUG*TT |
| | siVret sense | *GGCGUUCGAUAAUAUACUA*TT |
| | siVret antisense | *UAGUAUAUUAUCGAACGCC*TT |
| | siVret-L sense | *GCCAAACUGGCCAUGAUGA*TT |
| | siVret-L antisense | *UCAUCAUGGCCAGUUUGGC*TT |
| Others | 1U29 | *UCAAAAACUAACGGAUUGGUUUCGAACAG* |
| | 1U50 | *UCAAAAACUAACGGAUUGGUUUCGAACAGUCACCCGCCCGGACAGGUCCC* |
| | 1U80 | *UCAAAAACUAACGGAUUGGUUUCGAACAGUCACCCGCCCGGACAGGUCCC-*<br>*CUACCUGUCCCUAAUCAACUGGCAGCCGGG* |

＊RNA is shown in italic. L means left, forward. R means right, reverse

# 3. Results

# 3. Results

## 3.1. Knockdown of Trim or Nbr does not affect Siwi-piRISC maturation drastically

Trim and Nbr are exonuclease, which are the candidates of responsible factor for Siwi-piRISC maturation. To examine whether these factors are essential factors for Siwi-piRNA maturation, knockdown assays were performed. Flag-Siwi was expressed after knocking down Trim or Nbr in BmN4 cells (Fig. 8A). If either plays an important role in piRNA biogenesis, Siwi would be devoid of piRNA. Since, Papi was already identified as essential factor for Siwi-piRISC maturation, Papi-knockdown sample was experimented as control (Fig. 8A). Examination revealed that loss of Trim and Nbr little affected the levels of Siwi-loaded piRNAs whereas loss of Papi nearly completely abolished Siwi-piRNA loading (Figure 8B). This result suggests that papi is required, but Trim and Nbr are dispensable, for Siwi-piRNA production and piRISC formation in silkworm germline cells.

Although the levels of piRNAs loaded onto Flag-Siwi was little change by Trim loss, Siwi-piRNAs seemed to be slightly upshifted on RNA gels (Fig. 8B), as has been previously reported (Honda et al., 2013; Izumi et al., 2016). To examine the piRNA size more carefully, the RNA samples were run on a sequencing gel and RNA signals were quantified. The mean sizes of Siwi-piRNAs were 28.2 and 28.6 bases in control and Trim knockdown (kd) fractions, respectively (Fig. 8C). This mean that Siwi-piRNAs produced without Trim function is averagely 0.4nt longer than that from control cells. At present, the cause of this subtle, less than one nucleotide size difference induced by Trim loss remains unclear.

### 3.2. Depletion of Zuc accumulates piRNA intermediates in the Papi-Siwi complex

I then focused on Zuc, the rest of three candidate nucleases. Zuc has been shown to function in piRNA biogenesis in *Drosophila* (Ipsaro et al., 2012; Nishimasu et al., 2012) and is conserved among many species such as mice and silkworm. Flag-Siwi was expressed in Zuc-depleted BmN4 cells (Fig. 9A), and $^{32}$P-labeled RNAs that co-immunopurified with the proteins. Siwi was loaded with piRNAs at a much lower level than under normal conditions (Fig. 9B). Northern blotting confirmed that the levels of piRNAs abundantly found in Siwi-bound piRNA pools such as RT3-1 and piRNA-4 in normal (Nishida et al., 2009) severely decreased by Zuc depletion (Fig. 9C). Thus, Zuc is required for piRNA production in silkworm germline cells.

If Zuc is the factor processing the 3´ end of piRNA intermediates, Zuc knockdown should cause aberrantly accumulation of piRNA intermediates in the Papi-Siwi complex. To assess this possibility, the Papi-Siwi complex was immunopurified from Zuc-lacking BmN4 cells, and RNAs extracted from the complex were applied for northern blotting using a probe for RT3-1 piRNA. Examination revealed that RT3-1 piRNA intermediates strongly accumulated in the complex (Fig. 9D). On contrary, Trim depletion had little impact on the levels of piRNA intermediates in the complex (Fig. 9E), strengthening the idea that contribution of Trim to piRNA processing in BmN4 cells is trivial.

Papi and Zuc contain a MLS at the N-terminal end, whereas Trim has its MLS at the C-terminal end (Fig. 10A). Western blotting detected Papi, Zuc and Trim in the mitochondrial fractions of BmN4 cells (Fig. 10B). I then fractionated mitochondrial lysates on a sucrose density gradient and determined which fractions contain Papi, Zuc, and Trim, along with Siwi, by western blotting. Zuc and Papi were detected more strongly in #3-8 fractions than other fractions whereas Trim was relatively abundantly found in #10-13 fractions (Fig. 10C). I also performed immunoprecipitation from mitochondrial lysates, which showed that Zuc co-immunoprecipitated with Papi and Siwi (Fig. 10D). These results support the idea that Zuc physically interacts with the Papi-Siwi complex in 3´ end piRNA processing. Papi seems to offer a platform for facilitating piRNA processing in the germline cells by assembling necessary components to mitochondrial surface, namely piRNA-free Siwi, piRNA intermediates, Zuc endonuclease, and so on.

### 3.3. Zuc plays a role in the piRNA 3´ end formation *in vitro*

My results so far support the concept that 3´ end of piRNA intermediates within the PAPI-Siwi complex is processed by Zuc. To understand the properties of Zuc processing, I produced recombinant Zuc both wt and H141A mutant with no tag (Fig.

11A) and incubated at first with a naked RNA molecule of 50nt long (1U50) *in vitro*. The RNA substrate was $^{32}$P-labeled at its 5´ end. His141 of Zuc is located within the active site of the protein and alteration of the corresponding residue in *Drosophila* Zuc abolished its endonuclease activity (Nishimasu et al., 2012). Zuc wt, but not Zuc H141A mutant, fragmented the RNA substrate whose sizes range from 7 to 31 nt (Fig. 11B). The Zuc cleavage showed dose dependence (Fig. 11C). To perform Zuc treatment against substrate loaded onto Siwi, Flag-Siwi was immunopurified from BmN4 (Fig. 12A). When the substrate was loaded onto Flag-Siwi *in vitro* prior to Zuc treatment, the product size converged roughly between 27 to 31 nt, which are the sizes of endogenous mature piRNAs in BmN4 cells (Fig. 12B). Similar results were obtained when Flag-Siwi-substrate complex bound with immunoisolated Papi from BmN4 cells (Fig. 12C). To assess if Zuc processes endogenous piRNA intermediates in the Papi-Siwi complex to mature piRNAs in similar *in vitro* assays, the substrates were immunopurified from Zuc-depleted BmN4 cells using anti-Papi antibody and incubated with recombinant Zuc. Northern blotting showed that the RT3-1 piRNA intermediates within the complex were processed to mature RT3-1 piRNAs with Zuc wt, but not with Zuc H141A mutant (Fig. 13). These results confirm that Zuc is the 3´ end processor of piRNA intermediates in silkworm germ cells and Siwi protects 5´ end of piRNA intermediate and prevent Zuc from cleaving such region but Papi does not affect the pattern of cleavage.

I next wondered how the cleavage sites of Zuc are determined. To get the answer, I employed 1U80 RNA in the assays, the 5´ region of which is basically identical to 1U50 but the 3´ end had a 30nt extension. Prominent products appeared to be 35nt or shorter, while longer RNAs were barely detected (Fig. 14A). Interestingly, the cleavage pattern of 1U80 was very similar to that of 1U50 (Fig. 14B). The predicted structures of the two RNA molecules were different (data not shown), suggesting that high-dimensional structures have a low effect on Zuc cleavage. The product size was converged to 27~31 nt when the substrate was pre-bound with Siwi or the Papi-Siwi complex as in 1U50 case (Fig. 14C and 14D) raising possibility that there are sequence motif at 27~31 nt in the substrates for Zuc. To verify the possibility, I performed electrophoresis of cleavage products by Zuc with sequence gel (Fig. 15). RNA bands were classified to “strong”, “medium” and “weak” according to intensity of bands. Some properties of Zuc RNA cleavage emerged: 1) Zuc prefers to cleave RNA after pyrimidines (U and C) although the bias is not strict, 2) Zuc does not cleave G-rich region. These results suggest that the cleavage pattern by Zuc slightly depends on RNA sequence but Zuc does not have strict sequence motif. Protection of 5´ end of piRNA intermediates by Siwi is most important point to determine the length of piRNA.

Summarizing section 5.1 to 5.3, I concluded that Zuc is responsible nuclease for primary Siwi-piRNA production. Zuc cleaves Siwi-piRNA intermediate which is already loaded onto Siwi, to mature length on mitochondrial protein Papi (Fig. 16).

### 3.4. Ago3 interacts with Tudor protein Vreteno (Vret)

Above all, I elucidated the mechanism of antisense piRNA production in primary pathway. Then I tried to uncover Ago3-dependent antisense piRNA production in ping-pong cycle. First of all I conducted immunoprecipitation from BmN4 cell lysates using anti-Ago3 antibodies to identify the interactor of Ago3 to understand Ago3-dependent piRNA production. Silver-staining of the components revealed that 150 and 130 kDa proteins were co-immunoprecipitated with Ago3 (Fig. 17A). Both proteins were subjected to mass spectrometric analysis, which identified them as the silkworm homolog of *Drosophila* Vret essential for piRNA biogenesis in the ovaries (Handler et al., 2011; Zamparini et al., 2011). The closest homolog in mice and zebrafish is Tdrd1, which is also known to be essential for piRNA biogenesis in the gonads (Huang et al., 2011; Reuter et al., 2009; Vagin et al., 2009; Wang et al., 2009). To confirm the interaction between Ago3 and Vret, we raised an anti-Vret monoclonal antibody (Fig. 17B) and probed the immunoprecipitated materials with it. Vret was detected in the Ago3 complex (Fig. 17C). Previous studies showed that Vret/Tdrd1 interacts with PIWI members in flies (Piwi/Aub/Ago3), mice (Mili/Miwi2), and zebrafish (Zili/Ziwi) (Handler et al., 2011; Huang et al., 2011; Reuter et al., 2009; Vagin et al., 2009). Thus, the PIWI-Vret association is a species-conserved event.

Vret in the Ago3 complex appeared as two bands on western blots. Vret/Tdrd1 in flies (DmVret), mice (mTdrd1), and zebrafish (zTdrd1) was however detected as a single band on western blots (Huang et al., 2011; Reuter et al., 2009; Zamparini et al., 2011). Therefore, we speculated that the upper band (Vret-L in Fig. 17A) is full-length Vret, whereas the lower Vret-S is a degraded form of Vret-L. However, while cloning *Vret* cDNAs, we realized that BmN4 cells express two *Vret* mRNA isoforms. Comparison of the cDNA sequences revealed that they are distinct at the 5´ regions (Fig. 18A). The deduced peptide sequences showed that the longer cDNA encodes Vret consisting of one RNA recognition motif (RRM), one MYND family zinc-finger (ZnF-MYND), and two Tudor domains (Fig. 18B). The shorter one encodes Vret containing one ZnF-MYND and two Tudor domains but the RRM was not in there (Fig. 18B). We expressed both proteins in a His-tagged form in BmN4 cells, which co-migrated with endogenous Vret on western blots (Fig. 18C). A slight migration difference found between endogenous and exogenous Vret was due to the His-tag addition. Both Flag-Vret-L and -S co-immunoprecipitated with Ago3 as did endogenous Vret-L and -S (Fig. 18D).

### 3.5. Vret is necessary for secondary Siwi-piRISC production but dispensable for primary Siwi-piRISC production

I attempted to examine how loss of endogenous Vret impacts on piRNA biogenesis in BmN4 cells. Endogenous Vret was depleted by RNAi and Flag-Siwi and Flag-Ago3 were expressed individually in BmN4 cells. piRNAs were then isolated from both PIWI proteins and 5´-labeled with $^{32}$P-ATP. The abundance of piRNAs bound with Flag-Ago3 and Flag-Siwi were hardly changed (Fig. 19A). These results mean that Ago3-piRISC production which largely depends on the slicer activity of primary Siwi-piRISCs, had occurred properly even in the absence of Vret. I therefore suspected that Vret is necessary for secondary Siwi-piRISC production but unnecessary for primary Siwi-piRISC and Ago3-piRISC production.

To prove this, I performed northern blotting using probes that react to R2Bm- and Pao-piRNAs. R2Bm-piRNA was one of Siwi-bound piRNAs whose expression level was significantly reduced upon Ago3 loss in BmN4 cells (Nishida et al., 2015). In contrast, Pao-piRNA was one of Siwi-bound piRNAs whose expression level was increased by Ago3 loss in BmN4 cells (Nishida et al., 2015). Northern blotting showed that the level of R2Bm-piRNA, but that of Pao-piRNA was reduced by Vret loss (Fig. 19B). In addition, I deep-sequenced piRNAs loaded onto Flag-Siwi and Flag-Ago3 in normal and Vret-lacking BmN4 cells. A positive correlation was found between Ago3 and Vret depletions; namely, piRNAs reduced by Ago3 loss were downregulated by Vret loss while piRNAs increased by Ago3 loss were upregulated by Vret loss (Fig. 20). These results support our original notion that Vret is essential for secondary Siwi-piRISC production but dispensable for primary Siwi-piRISC production. DmVret was shown to be necessary for primary piRNA biogenesis in both ovarian somatic and germ cells (Handler et al., 2011; Zamparini et al., 2011) (Fig. 21A). Tdrd1 in mice was reported to be essential for first half of ping-pong cycle (Reuter et al., 2009; Vagin et al., 2009) (Fig. 21B) whereas Tdrd1 in zebrafish was shown to be necessary for second half of ping-pong cycle (Huang et al., 2011) (Fig. 21C). Functional phase of Vret in piRNA biogenesis seems to be different among species however Vret/Tdrd1 plays an essential role for antisense piRNA biogenesis in the all species interestingly.

### 3.6. The RNA-binding activity of Vret is dispensable for secondary Siwi-piRISC production

Species-conserved function of Vret/Tdrd1 for antisense piRNA production raised possibility that Vret recognize antisense TE transcript with RNA binding activity. RRM confers the RNA-binding activity to host proteins. Therefore, I inferred that Vret-L containing RRM, but not Vret-S, accommodates the RNA-binding activity and only Vret-L is functional form. As expected, crosslink immunoprecipitation (CLIP) experiments showed that Vret-L, but not Vret-S, bound with endogenous RNAs *in vivo* (Fig. 22A). Simultaneous deletion of Vret-L and -S induced reduction of R2Bm Siwi-piRNA (Fig. 19B). In contrast, single depletion of Vret-L hardly changed the level of R2Bm-piRNA unexpectedly (Fig. 22B). This finding suggests that the RNA-binding activity of Vret-L through RRM is dispensable for piRNA biogenesis in BmN4 cells.

According to InterPro's domain prediction, DmVret has only two Tudor domains and Tdrd1 in mice and zebrafish have one ZnF-MYND and four Tudor domains but lack RRM (Fig. 22C). Thus, RNA binding activity of Vret should not be necessary for piRNA production from evolutional point of view.

### 3.7. Vret interconnects Ago3-piRISC with apo-Siwi through sDMA modification

Next I focused on protein-protein interaction between Vret and PIWI proteins. Vasa displaces cleaved RNAs from Siwi-piRISCs to facilitate the RNA loading onto Ago3 (Nishida et al., 2015). For this, Vasa interconnects Siwi-piRISC with apo-Ago3. In this study, I found that Vret functions in secondary Siwi-piRISC production and so speculated that Vret interconnects Siwi-piRISC with apo-Ago3. To examine this possibility, I isolated RNAs from the Vret-L/Ago3 complex and probed them for PiggyBac-piRNA, the representative of Ago3-bound piRNAs (Nishida et al., 2015). More PiggyBac-piRNAs were detected in Vret-L/Ago3 complex than in Ago3 only (Fig. 23A), suggesting large number of Vret-binding Ago3s are in piRISC form. However, RT3-piRNA, the representative of Siwi-bound piRNAs, was not detected in the Vret-L complex (Fig. 23B). These results indicate that Vret interconnects Ago3-piRISC and apo-Siwi to facilitate secondary Siwi-piRISC production.

Tudor domains, if not all, exhibit the sDMA-binding activity and the association with sDMA-containing proteins requires aromatic cage residues and an asparagine nearby (Liu et al., 2010). In this study, I tested whether Vret binding Siwi and Ago3 requires PIWI's sDMA modification. For this, I used sDMA-modification-defective RK mutants of Siwi and Ago3 (Nishida et al., 2018). Both mutants failed to co-purify with Vret in contrast to WT controls (Fig. 23C). Thus, Vret-PIWI interaction is also sDMA-dependent. To ask which of the two Tud domains in Vret is responsible for Siwi and Ago3 binding, we produced two Vret mutants, Tud1mut and Tud2mut, where three conserved residues in each mutant were mutated to alanines (Fig. 24A). Immunoprecipitation showed that Tud1mut only weakly associated with Siwi and Ago3, while Tud2mut bound both PIWI proteins as well as WT did (Fig. 24B). These results indicate that Vret binds Siwi and Ago3 through the N-terminal Tudor domain. In this assay, Flag-Vret-L co-immunopurified with endogenous Vret-S along with Siwi and Ago3 (Fig. 24B). Vret might form a high-ordered structure with not only apo-Siwi and Ago3-piRISC but also Vret itself (Fig. 24C).

### 3.8. Ago3-piRISC and Vret collaboratively assemble Ago3 bodies

Siwi and Ago3 are localized to nuage, germ cell-specific, perinuclear non-membranous structures. Immunofluorescent analysis showed that Vret mostly localizes to Ago3-positive nuage but only partially to Siwi-positive nuage (Fig. 25A and 25B). Exogenous Vret-L and Vret-S co-localized also with Ago3-positive nuage (Fig. 25C). These results may agree with the observations that Vret tightly bound with Ago3 but only weakly with Siwi (Fig. 25D). Our previous study showed that Vasa signals greatly overlapped with Siwi signals (Nishida et al., 2015). These results also support the idea that the functions of Vret and Vasa are distinct in the piRNA pathway.

In the absence of Vret, Ago3 failed to localize to nuage but scattered broadly in the cytosol (Fig. 26A). Loss of Ago3 also caused Vret being scattered in the cytosol (Fig. 26B). Thus, Vret and Ago3 collaboratively assemble the Ago3-positive nuage. Siwi-positive nuage was still present in both cases, although the number was lower than that in normal cells (Fig. 26C and 26D). This suggests that Siwi-positive nuage is not uniform and that some fraction of Siwi localizes to Ago3-positive nuage. I hereinafter refer to Ago3-positive nuage as Ago3 bodies. Ago3 co-immunoprecipitation (co-IP) from Vret depleted BmN4 showed Ago3-Siwi interaction got much weaker without Vret (Fig. 27A). Flag-Vret-L co-IP from Ago3 depleted and Flag-Vret-L transfected cells revealed Flag-L-Siwi interaction got much weaker without Ago3 (Fig. 27B). These results suggest appropriate localization at Ago3-bodies of Vret and Ago3 is necessary to make Ago3-Vret-Siwi complex.

Vret prefers to bind Ago3 in its piRISC form; thus, I inferred that piRNA loading onto Ago3 may be necessary for Ago3-body assembly. To assess this, I produced Ago3 KA mutant, in which Lys637 was mutated to alanine. The Ago3 KA mutant failed to bind piRNAs (Fig. 28A) as did the equivalent mutant of Siwi (*i.e.,* K611A) (Matsumoto et al., 2016). I also produced Ago3 DDH mutant, where the active center, *i.e.,* the DDH motif composed of Asp597, Asp767, and His901, was substituted with three alanines. This mutant should be defective in target RNA cleavage although the piRNA binding activity should be maintained. Indeed, the DDH mutant was loaded with piRNAs as well as WT (Fig. 28A).

I found that the piRNA binding-defective Ago3 KA mutant failed to localize at Ago3 bodies in normal BmN4 cells (Fig. 28B). In contrast, the slicer-defective DDH mutant was localized to Ago3 bodies as well as WT (Fig. 28B). These results strongly suggest that Ago3 localization to Ago3 bodies is piRNA-dependent. I then expressed Ago3 KA and DDH mutants individually in Ago3-depleted BmN4 cells; namely, under conditions where no Ago3 bodies were initially formed although Vret was still present. Both mutants were able to bind Vret (Fig. 28C). However, the DDH mutant but not KA mutant formed Ago3 bodies (Fig. 28D). These results strongly suggest that the existence of Ago3 and Vret in the cells is insufficient but RNA targeting of Ago3-piRISCs is also required to assemble Ago3 bodies.

### 3.9. Lack of Siwi increases the level of Ago3 phosphorylation and enlarges Ago3 bodies

To explore how Siwi loss impacts Ago3-body formation, immunofluorescence was conducted upon Siwi depletion. Interestingly, in the absence of Siwi, Ago3 bodies looked abnormally enlarged (Fig. 29A). Immunostaining with anti-Vret antibodies detected Vret in the enlarged bodies (Fig. 29B). These results suggest that loss of Siwi enlarged Ago3 bodies where Ago3-piRISCs and Vret were encapsulated.

Western blotting revealed that Ago3 can be detected as a doublet upon Siwi loss [see “Total” lanes in Siwi knockdown (KD) in Fig. 29C]. The size difference was about several kDa. I then fractionated the total lysates by centrifugation at 17,000 x *g* and performed western blotting: The lower band in both +/- Siwi KD samples was detected into the supernatant, whereas the upper band in the Siwi KD sample remained in the pellet fraction (Fig. 29C). These findings indicate that loss of Siwi drastically changed the property of Ago3 *in vivo*. I speculated that the Ago3 mobility shift may be due to phosphorylation. To assess this, I performed phosphatase treatment against Immunoisolated Ago3 from the pellet. Western blotting shows Ago3 after the treatment was detected as a single band as Ago3 in normal cells (Fig. 29D). These findings indicate that loss of Siwi induced Ago3 phosphorylation and that this post-translational modification is the cause of changes in the property of Ago3.

To identify the phosphorylation sites in phosphorylated Ago3 (P-Ago3), I prepared Siwi-lacking BmN4 lysates in a harsh buffer containing Empigen and conducted immunoprecipitation using anti-Ago3 antibodies. The materials obtained were forwarded for silver-staining (Fig. 30A) and mass spectrometric analysis. The latter experiment revealed that the Ago3 phosphorylation sites were Ser112, Ser117, Ser143, and Ser149 (Fig. 30B). These residues were not conserved among species; thus, Ago3 phosphorylation may be unique to silkworm Ago3 (Fig. 30C). I altered all four serine residues to alanines and assessed if the mutation abrogates Ago3 phosphorylation. However, P-Ago3 was still detectable, albeit minor, in Siwi-depleted cells (Fig. 31A). Some kinases are known to phosphorylate flanking residues when *bona fide* target sites were not available. Thereby, I additionally mutated Ser116, Ser140, Ser145 and Ser150 to produce Ago3 8SA mutant (Fig. 30B). The band shift was hardly observed for the 8SA mutant in Siwi-depleted cells (Fig. 31B). I hereinafter use this 8SA mutant as a phosphorylation-defective Ago3 mutant.

I next examined how Ago3 phosphorylation is important for piRNA biogenesis in BmN4 cells. For this, I ectopic expressed the 8SA mutant in BmN4 cells where endogenous Ago3 had been depleted. The reduced R2Bm-piRNA level caused by Ago3 loss was restored by the expression of 8SA mutant as well as that of Ago3 WT (Fig. 32). Ago3 phosphorylation seems unnecessary for piRNA production in BmN4 cells. Nonetheless, to understand at which step in the pathway, Ago3 is phosphorylated, I examined the phosphorylation status of Ago3 DDH and KA mutants. The DDH mutant appeared as a doublet upon Siwi depletion as did WT, although the KA mutant was detected as a single band (Fig. 33A). These results indicate that Ago3 phosphorylation most likely occurs upon Ago3-piRISC formation. In BmN4 cells where Vret was co-depleted along with Siwi, Ago3 phosphorylation was little detected (Fig. 33B). This suggests that the Ago3 post-translational modification occurs upon Ago3 body assembly with Vret. It is noted that the expression level of KA mutant was much lower than that of DDH mutant; this might be due to the failure of KA mutant in piRNA loading. I noticed that P-Ago3 was also detected in control cells, albeit minor (see the far-left lane on the longer exposure panel in Fig. 33A). This indicates that Ago3 may undergo phosphorylation/dephosphorylation loop even in regular BmN4 cells. Because the 8SA mutant fully restored the defect in piRNA biogenesis caused by loss of endogenous Ago3 (Fig. 32), we currently have no clue what the biological significance of Ago3 undergoing phosphorylation/dephosphorylation loop is. Alternative idea is that P-Ago3 is degraded upon phosphorylation for turnover and dephosphorylation never occur to P-Ago3.

### 3.10. Ago3-piRISC remains tightly bound with cleaved target RNAs in the absence of Siwi

The KA mutant was dispersed among cytoplasm (Fig. 28B). Therefore, lack of Siwi causes Ago3 aggregated in its piRISC form, which was accompanied by Vret. I then speculated that the aggregates might also contain Ago3-target RNAs. To test this possibility, I isolated RNAs from Ago3 (in a mixture of unphosphorylated and phosphorylated) immunoisolated from Siwi-depleted cells (Fig. 30A) and $^{32}$P-labeled them. The result suggested that Ago3 in Siwi-lacking cells is loaded with piRNAs as in control cells (Fig. 34A). Interestingly, the amount of Ago3-loaded piRNAs was higher in Siwi-depleted cells than that in normal cells, although the abundances of Ago3 immunoisolated were nearly equal under Siwi +/- conditions (Fig. 34A). piRNAs may remain stuck on Ago3 in the absence of Siwi, although at this moment the biological relevance of the incident remains unknown.

A discrete 16 nt band was also detected on the blot in the absence of Siwi (Fig. 34A). I isolated RNAs migrating around the region from the gel and sequenced them. After extracting sequence reads corresponding to silkworm transposons (gifted by Dr. Shinpei Kawaoka), I analyzed them computationally. This revealed that 80.4% of the sequence reads correspond to antisense oligos to transposons mRNAs (Fig. 34B). The size distribution confirmed that the most abundant size was 16 nt (Fig. 34C). I examined the distance between the 3′ end of 16 nt RNAs and the 5′ end of Ago3-bound piRNAs. The most abundant distance was 10 nt (Fig. 34D). The “10 nt distance” is exactly equal to the distance between the 5′ end of Ago3-bound piRNAs and the 5′ end of Siwi-bound piRNAs produced through the ping-pong cycle (Fig. 34D). These suggest that the 16 nt RNAs are bi-products of Ago3-piRISC-mediated target RNA cleavage and I hereinafter call these RNAs Target-Ss (Fig. 34E) (Xiol et al., 2012). Interestingly, Siwi/Vret double knockdown reduced Target-S associating with Ago3 (Fig.35). Regarding Target-Ss as footprints of target RNA, this data strongly suggests Vret plays an essential role for target-binding ~ target-cleavage.

Northern blotting on RNAs isolated from the Ago3 complex using a probe reacting to *Bmmar6*-piRNA, which is one of the most abundant antisense piRNAs loaded onto Siwi, revealed the presence of piRNA precursors in the RNA pool (Fig. 36A). I isolated 50-100 nt long RNAs from the gel and determined their sequences. I again extracted sequence reads corresponding to transposons and analyzed them computationally. It was found that they were mostly transposon RNAs in antisense orientation (88.6%) (Fig. 36B). The size distribution analysis showed that 52 nt was the most abundant (Fig. 36C), although the relevance of the finding remains vague. Examination of the distance between the 5′ end of Ago3-bound piRNAs and the 5′ end of those antisense piRNA precursors showed that the distance was mostly 10 nt (Fig. 36D). This means that these RNAs and Target-Ss correspond to target RNAs just cleaved by Ago3-piRISCs but not evicted from the piRISCs and so remaining on the complex (Fig. 36E). Hereafter, I call the longer target RNAs Target-L. Since Target-L and -S were derived from variety of transposons (Fig. 37), 10 nt overlaps showing at Fig. 34D and 36D did not reflect the pattern of a few kinds of abundant sequences.

### 3.11. Ago3-piRISCs produce Siwi-piRNA intermediate tandemly

Phasing analyses can calculate distance between 3´ ends of upstream sequences and 5´ ends of adjacent downstream sequences used to see phased-piRNAs (Han et al., 2015; Mohn et al., 2015). Phasing analyses also revealed that Papi-binding int-piRNAs are yielded tandemly and this pattern may be dependent on cleavage by Ago3-piRISCs (Nishida et al., 2018). I utilized this analysis and found that Target-Ls are phased (Fig. 38). 3´ ends of Target-Ss tend to be mapped on 1nt upstream of 5´ ends of Target-Ls (Fig. 39) but not vice versa (Fig. 40). Target-Ss are not tandemly produced (Fig. 41). Since Target-Ls/Ss are derived from variety of transposons (Fig. 37), production patterns of them are not dependent on limited number of dominant sequences.

Half amount of 5´ ends are shared between Target-Ls and Siwi-piRNAs (Nishida et al., 2015) (Fig. 42A) and 5´ends of Target-Ls are aligned to Papi-binding int-piRNA at almost same rate (Fig. 42B). These informatic data above suggest that Ago3-piRISCs produce Siwi-int-piRNA tandemly from a piRNA precursor and no more cleavage products are tandemly produced from upstream region after a Target-S are produced at 5´ side of a piRNA precursor (Fig. 42C). Target-Ls may be loaded onto Siwi by Vasa-like helicase as Siwi-int-piRNAs and processed on Papi.

Summarizing 3.4~3.11, Ago3-piRISCs produce Siwi-piRNA intermediates tandemly anchored at nuage by Vret (Fig. 43).

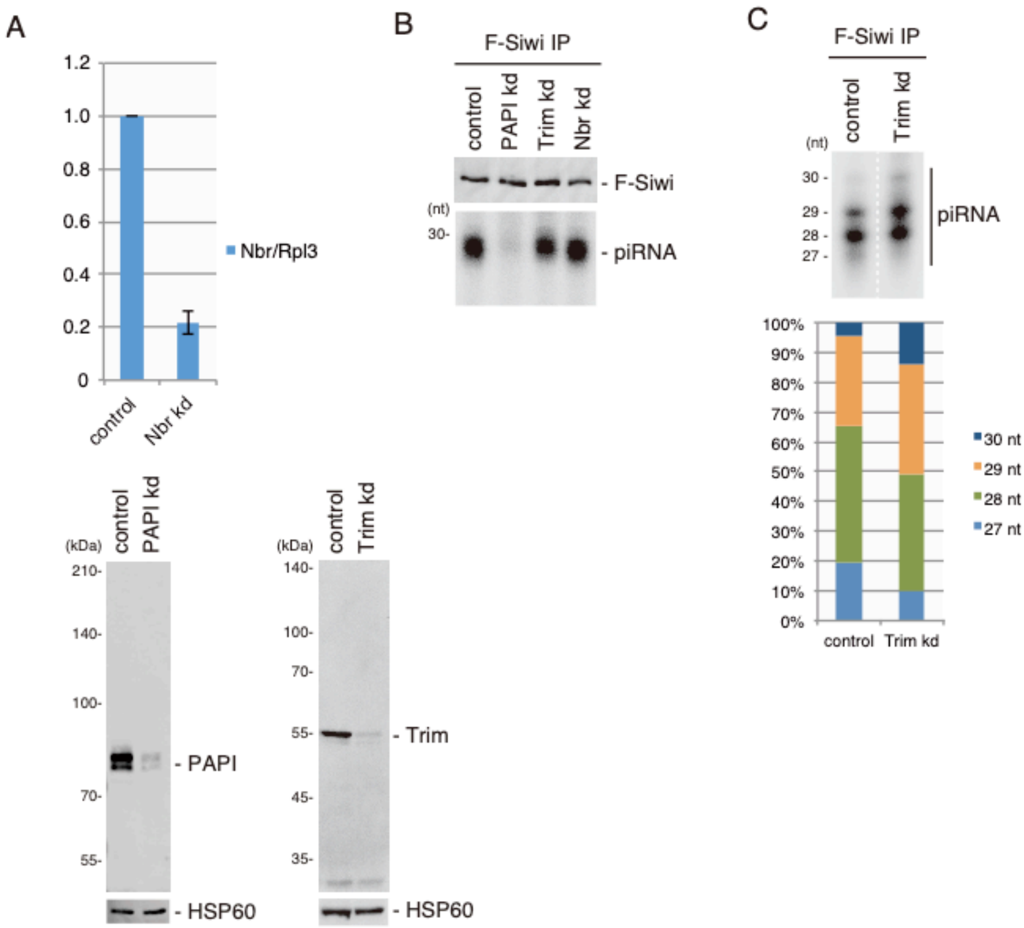


**Fig. 8. Depletion of Trim or Nbr does not strongly affect Siwi-piRNA biogenesis**

(A) RT-qPCR showed *nbr* is reduced at mRNA level by *nbr* RNAi. Western blotting reveals Papi and Trim are reduced at protein level. (B) Knockdown of Trim and Nbr do not change the amount of Siwi-piRNA in contrast to Papi kd. (C) piRNAs appear to be slightly longer when Trim is depleted.

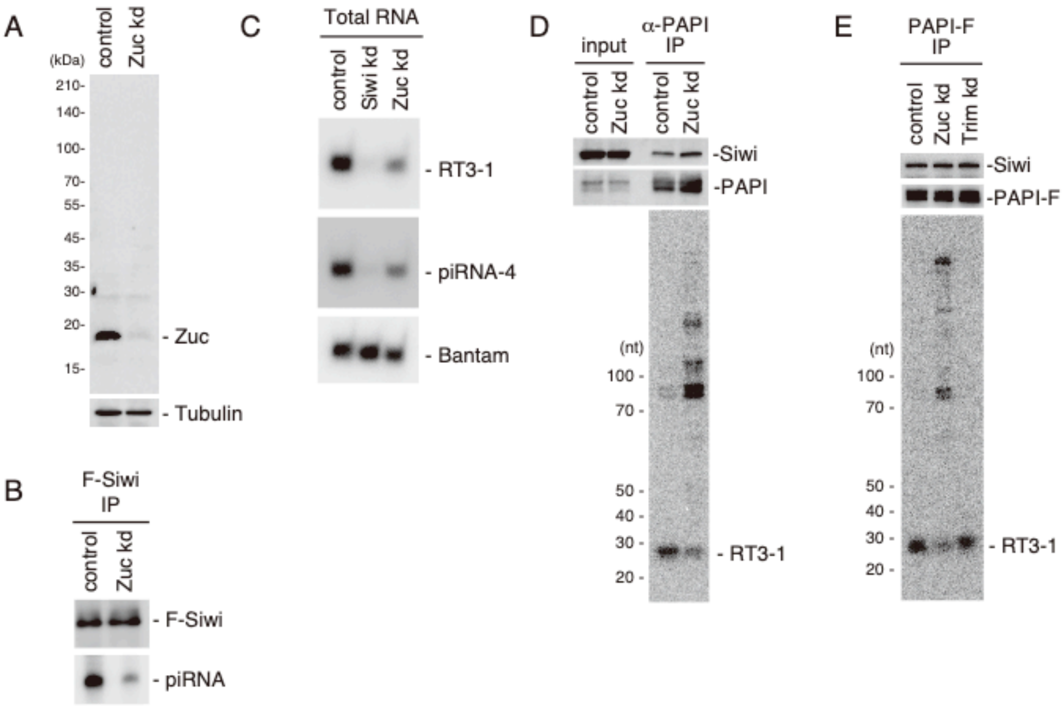


**Fig. 9. Depletion of Zuc induces loss of mature Siwi-piRNA and accumulation of Siwi-piRNA intermediate**

(A) Western blotting shows Zuc is well reduced at protein level. (B) Knockdown of Zuc radically reduced the amount of Siwi-piRNA. (C) Northern blotting reveals Siwi-piRNA named RT3-1 and piRNA-4 are reduced by Zuc kd. Bantam is miRNA used as loading control here. (D) RT-3 Siwi-piRNA intermediates are accumulated on Papi-Siwi complex in Zuc-depleted BmN4. (E) Deletion of Trim does not induce accumulation of RT-3 Siwi-piRNA intermediates on Papi-Siwi complex.

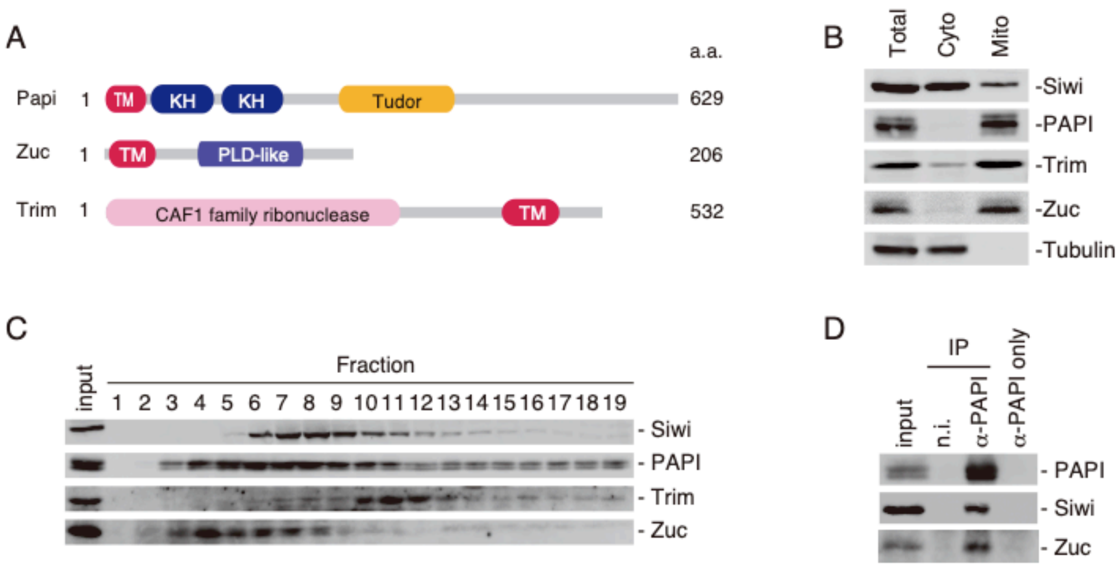


**Fig. 10. Zuc is involved in Papi-Siwi complex.**

(A) Domain structures of Papi, Zuc and Trim. All the three genes have transmembrane region to be localized at mitochondrion. (B) Siwi, Papi, Trim and Zuc are involved in mitochondria fraction. (C) Sucrose density gradient centrifugation shows Siwi, Papi and Zuc are involved in the same fraction (#6~8) but Trim is in fraction #10~12 abundantly. (D) Siwi and Zuc are involved in Papi immunoprecipitate.

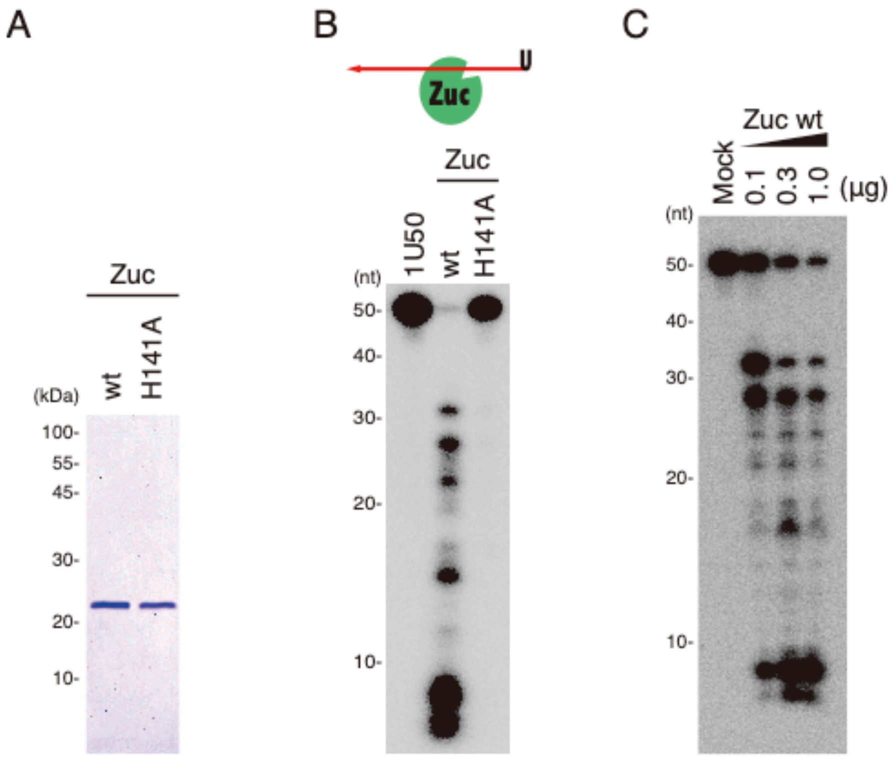


**Fig. 11. Recombinant Zuc cleaves 50nt RNA substrate**

(A) Zuc wild-type (wt) and catalytic mutant, H141A, with no tag are purified. (B) Only Zuc wt cleave 50nt RNA substrate (1U50) labeled with $^{32}$P at 5´ end but H141A does not suggesting H141A works as negative control. (C) Zuc cleaves RNA substrate dose-dependently.

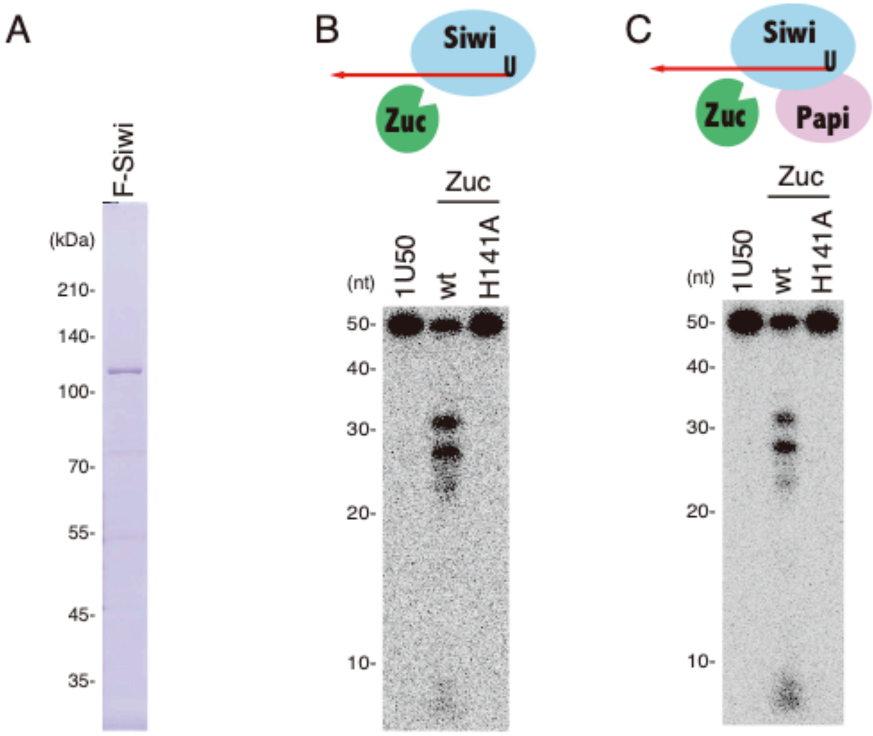


**Fig. 12. Zuc processes 1U50 RNA to length of mature piRNA**

(A) Flag-Siwi (F-Siwi) is immunopurified with Flag monoclonal antibody from F-siwi transfected BmN4. (B) $^{32}$P-labeled 1U50 is incubated with immunopurified F-Siwi. 1U50 associated with F-Siwi is process to 27~31 nt which is the length of mature Siwi-piRNA. (C) 1U50 associated with F-Siwi is pre-incubated with immunoisolated endogenous Papi. 1U50 associated with F-Siwi and Papi is process to 27~31 nt, which is the length of mature Siwi-piRNA.

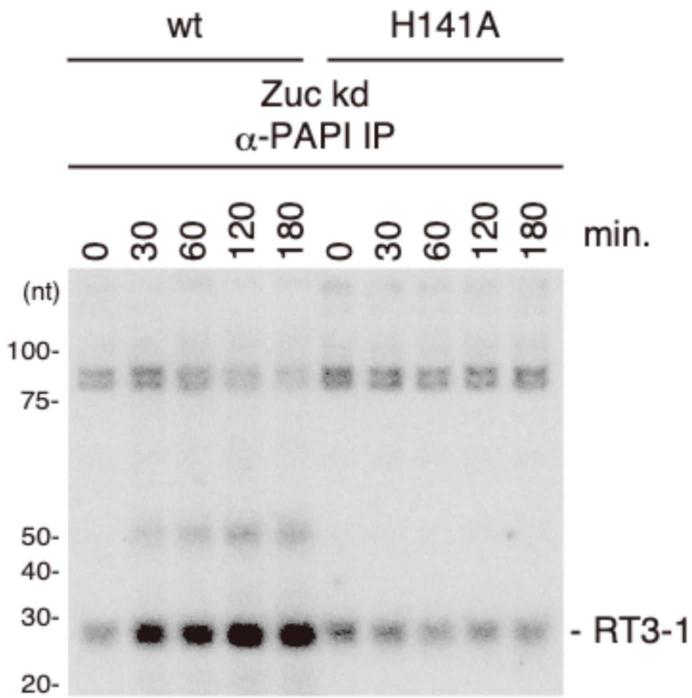


**Fig. 13. Zuc processes endogenous RT3-1 Siwi-piRNA intermediate in Papi complex to mature piRNA**

Papi complex is immunoisolated from Zuc depleted BmN4. Papi complex and recombinant Zuc are mixed *in vitro* and then RNAs are isolated from the complex. Northern blotting shows RT3-1 Siwi-piRNA intermediate is processed to mature length by Zuc wt trearment.

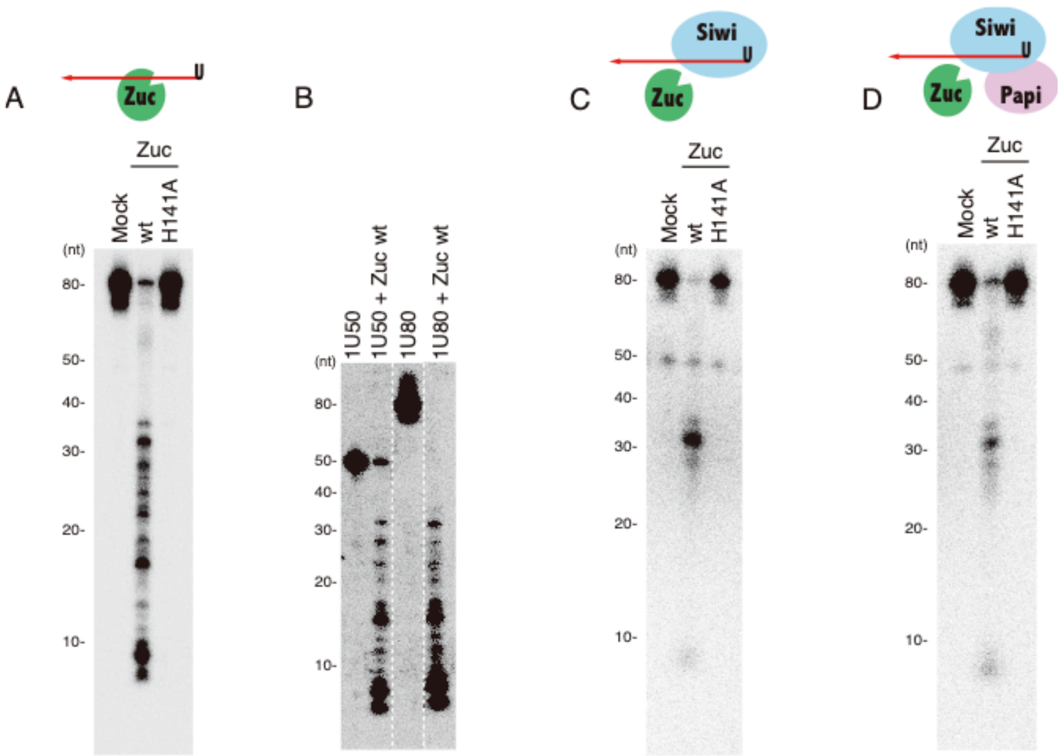


**Fig. 14. Zuc processes 80nt RNA substrate (1U80) to mature length as 1U50**

(A) Only Zuc wt cleave 80nt RNA substrate (1U80) labeled with $^{32}$P at 5´ end but H141A does not. (B) Zuc produces similar cleavage products in both 1U50 and 1U80 cases. (C) $^{32}$P-labeled 1U80 is incubated with immunopurified F-Siwi. 1U80 associated with F-Siwi is process to 27~31 nt which is the length of mature Siwi-piRNA. (D) 1U80 associated with F-Siwi is pre-incubated with immunoisolated endogenous Papi. 1U80 associated with F-Siwi and Papi is process to 27~31 nt which is the length of mature Siwi-piRNA.

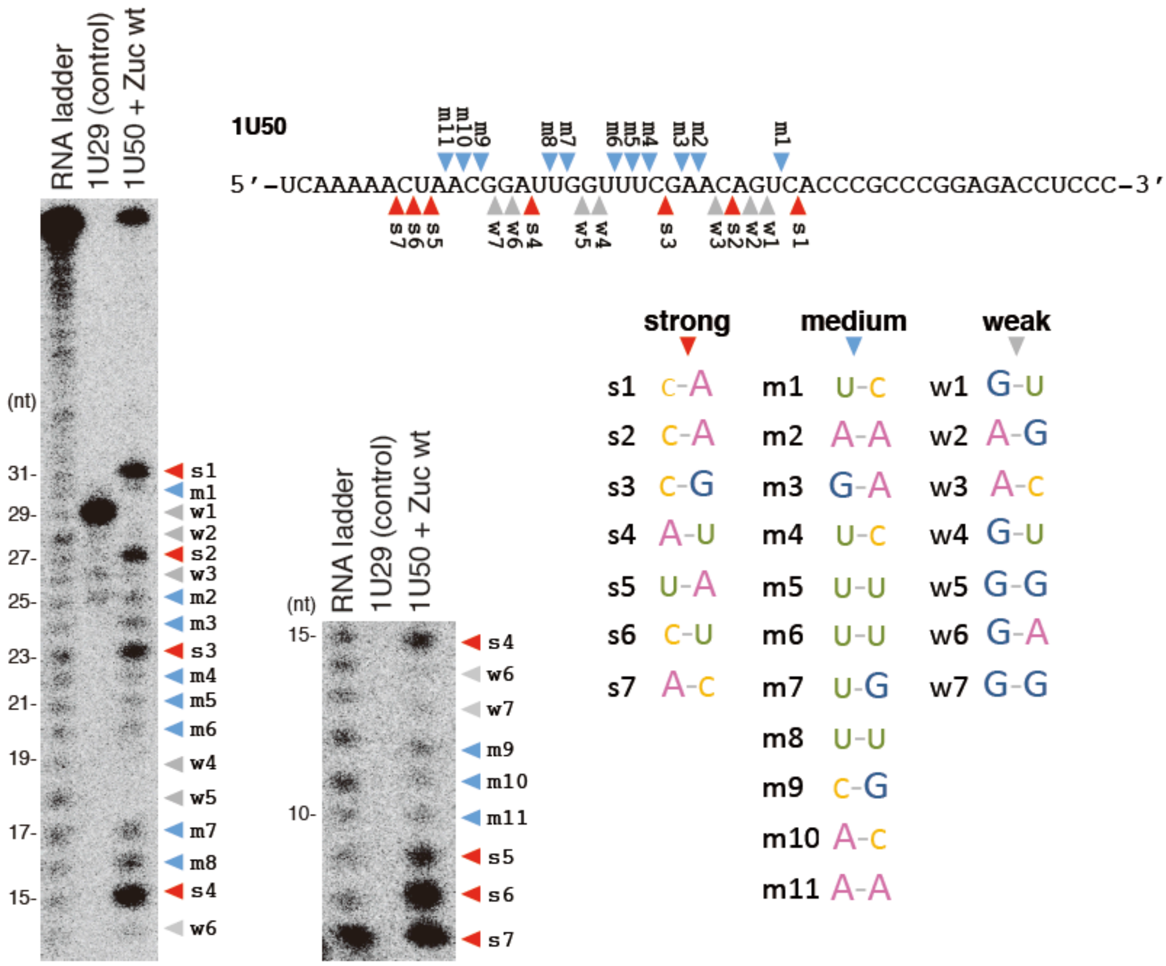


**Fig. 15. Zuc does not show nucleotide preference**

Upon Zuc treatment against 1U50, RNAs are electrophoresed with sequence gel. 1U29, 29nt RNA, which has the same sequence as 1U50's 1~29nt region, is used as size marker. RNA bands are classified to three types, strong, medium and weak, according to intensity of the bands with ImageJ. There are no strong preferences in cleavage pattern.

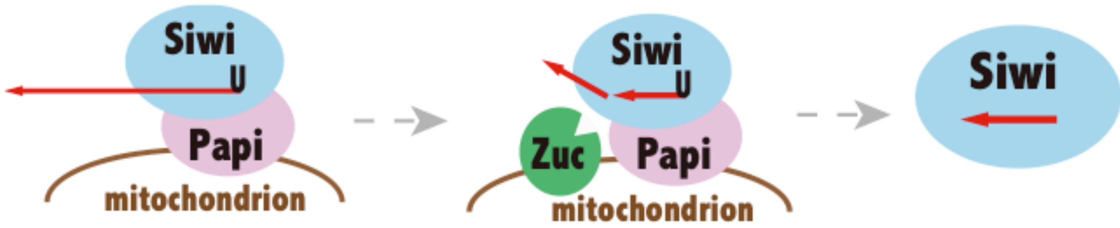


**Fig. 16. Model of primary piRNA biogenesis in *Bombyx***

piRNA intermediate is loaded onto Papi-binding Siwi on mitochondrion. Zuc cleaves Siwi-piRNA intermediate at 3´ side not protected by Siwi for maturation.

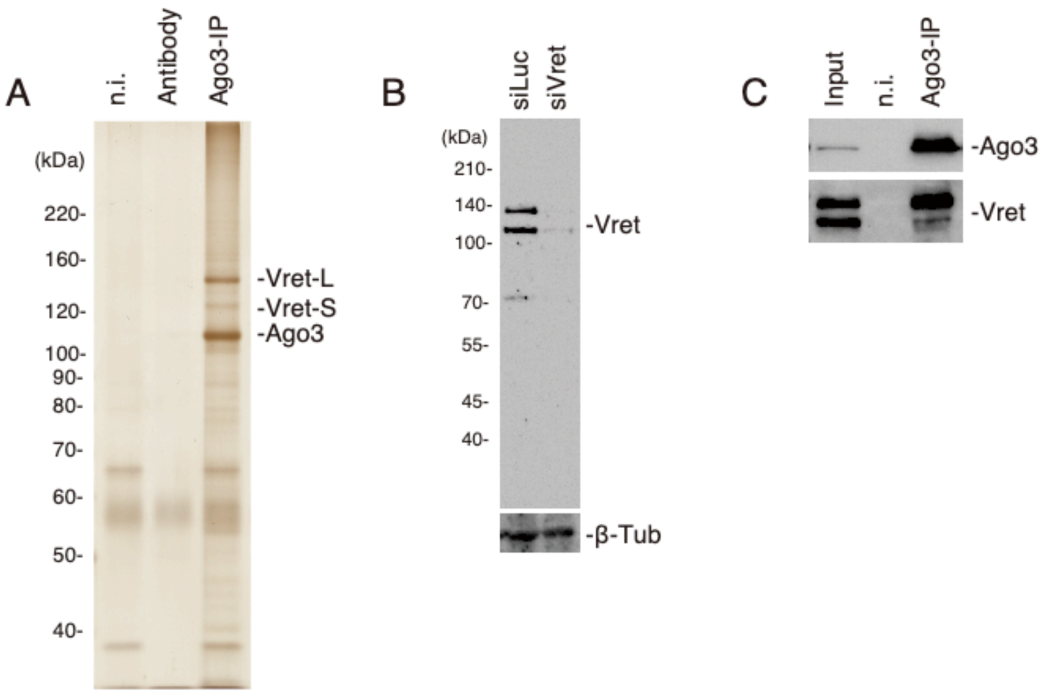


**Fig. 17. Vret associates with Ago3**

(A) Silver staining of protein components in the Ago3 complex immunoisolated from BmN4 cells. (B) Western blotting shows the specificity of anti-Vret monoclonal antibody raised in this study. β-Tub and tubulin were used as loading controls. (C) Western blotting showing the presence of Vret in the Ago3 complex in (A).

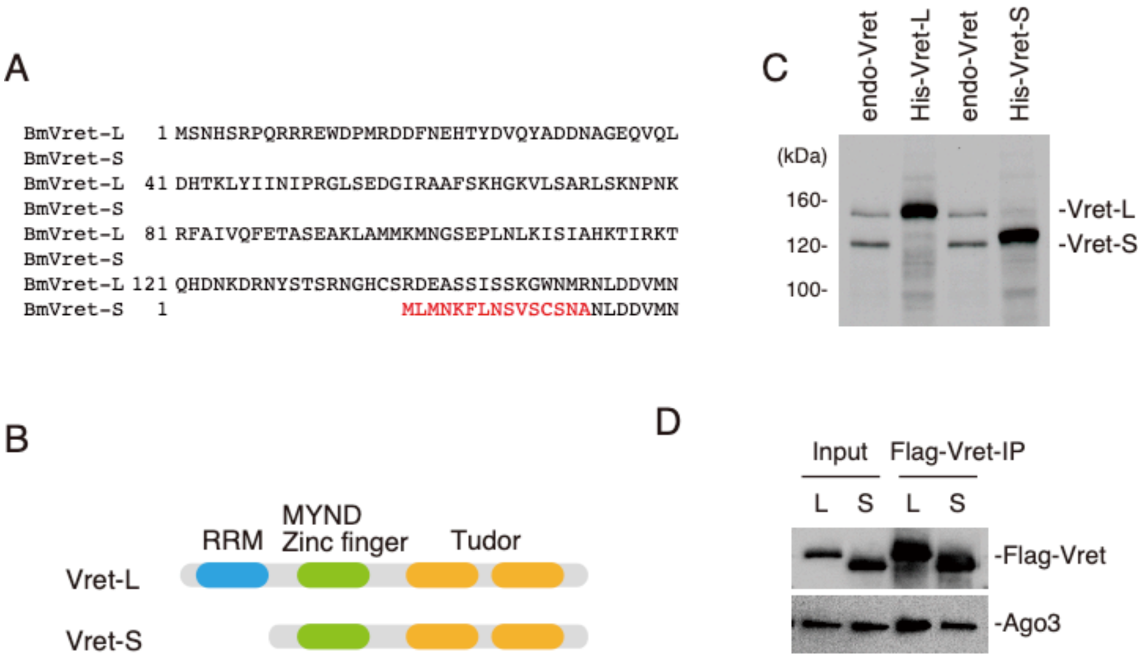


**Fig. 18. Two isoforms are expressed in BmN4**

(A) Sequence Alignment of N terminal region of BmVrets. The figure was prepared using Clustal Omega (http://www.ebi.ac.uk/Tools/msa/clustalo). Red letters indicates Vret-S specific sequence. (B) Domain structures of Vret-L and -S predicted by InterPro (https://www.ebi.ac.uk/interpro/). Vret-L contains RNA recognition motif (RRM), one MYND family zinc-finger (ZnF-MYND), and two Tudor domains. Vret-S lacks RRM. (C) Western blotting of immunoisolated endogenous Vret (endo-Vret) and *in vitro* translated His-Vrets. (D) Western blotting shows Flag-Vret-L/S both associates with Ago3.

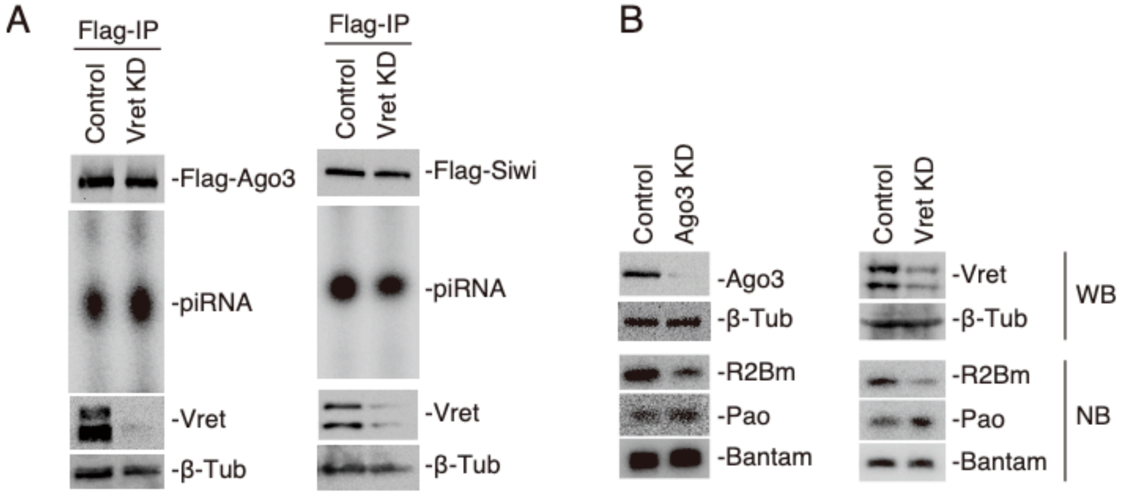


**Fig. 19. Vret is necessary for Ago3-dependent Siwi-piRNA production**

(A) RNAs co-immunoprecipitated with Flag-Siwi and Flag-Ago3 are visualized by $^{32}P$ labelling. Western blotting shows Flag-Siwi and Flag-Ago3 are immunoprecipitated at the same level and Vret was successfully reduced. (B) Northern blotting shows knockdown of Vret induce reduction of an Ago3-dependent Siwi-piRNA named R2Bm and increase of Ago3-independent, primary pathway dependent in other words, Siwi-piRNA named Pao.

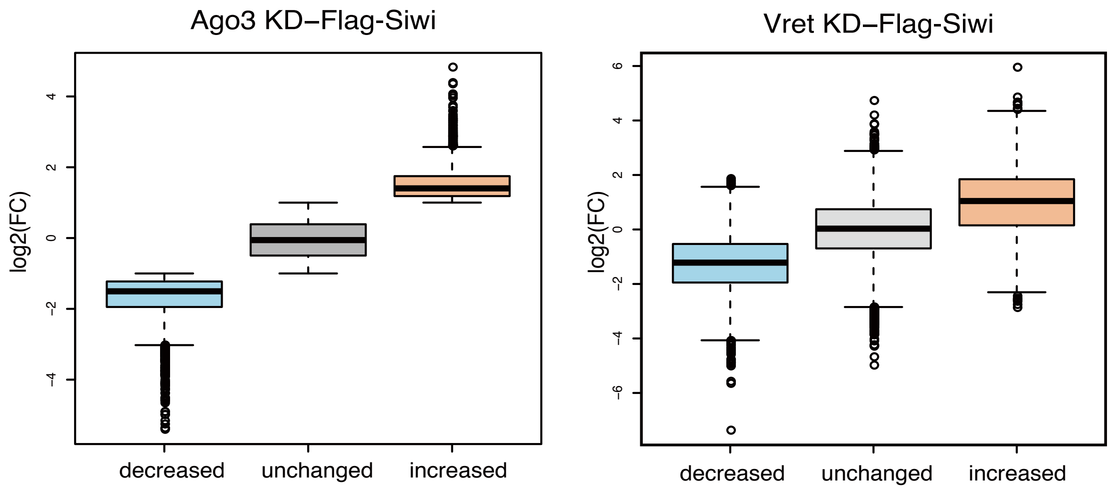


**Fig. 20 Ago3 dependent Siwi-piRNAs are reduced by Vret depletion**

In left panel, piRNAs from control and Ago3-depleted BmN4 are compared and categorized into three types (Ago3 KD/Control < 1/2: “decreased”, 1/2 < Ago3 KD/Control < 2: “unchanged”, Ago3 KD/Control > 2: “increased”). Right panel shows “decreased” piRNAs are decreased by Vret KD and “increased” piRNAs are increased by Vret KD.

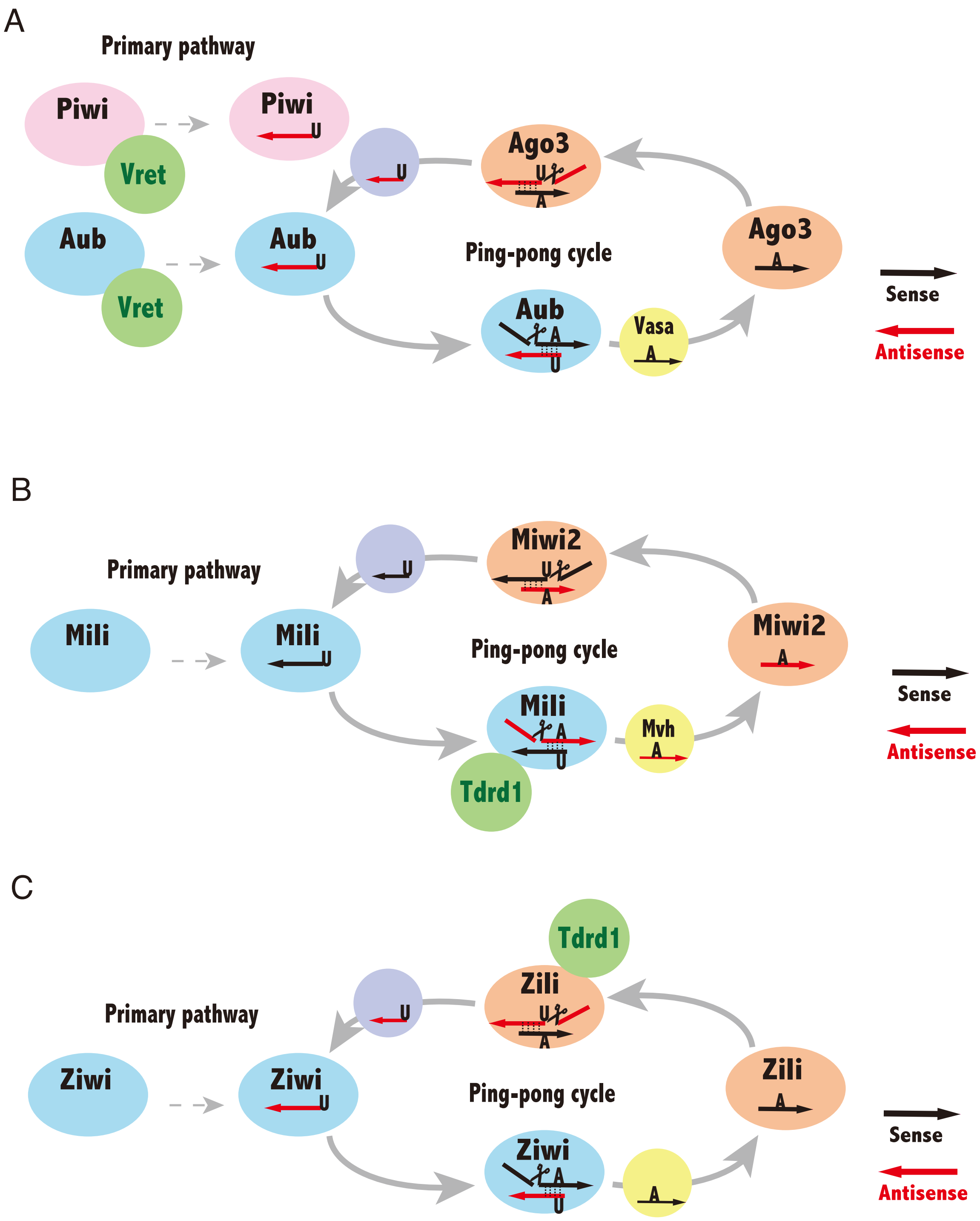


**Fig. 21 Functional phase of Vret in piRNA biogenesis is reported to be different among species**

(A) piRNA biogenesis model in *Drosophila*. Previous researches mentioned Vret play a role for primary piRNA biogenesis (Handler et al., 2011; Zamparini et al., 2011). (B) piRNA biogenesis model in mice. Previous researches mentioned Tdrd1 is important for first half of ping-pong cycle (Reuter et al., 2009; Vagin et al., 2009). (C) piRNA biogenesis model in zebrafish. Previous research mentioned Tdrd1 is important for second half of ping-pong cycle (Huang et al., 2011).

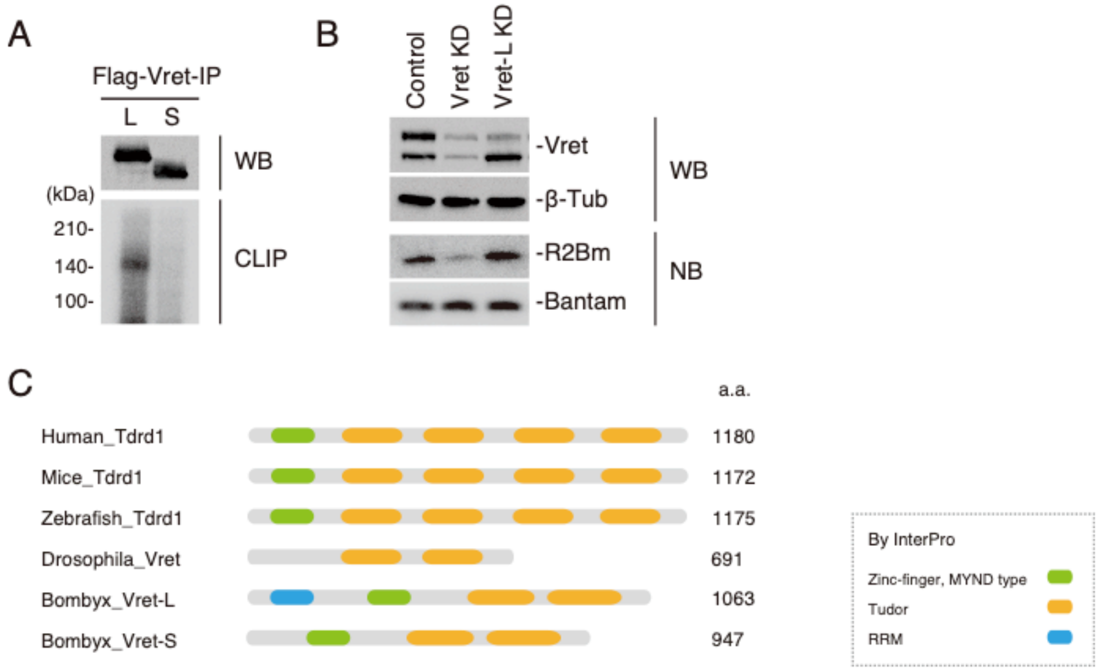


**Fig. 22. RRM of Vret is dispensable for piRNA biogenesis.**

(A) RNAs co-immunoprecipitated with Flag-Vret-L/S are labeled according to CLIP method. CLIP results shows Flag-Vret-L specifically associates with RNAs. (B) Northern blotting with probe for R2Bm, a typical Ago3-dependent Siwi-piRNA, indicates single knockdown of Vret-L does not affect R2Bm Siwi-piRNA production. (C) Domain structure of Vrets/Tdrd1s in several animals predicted by InterPro (https://www.ebi.ac.uk/interpro/).

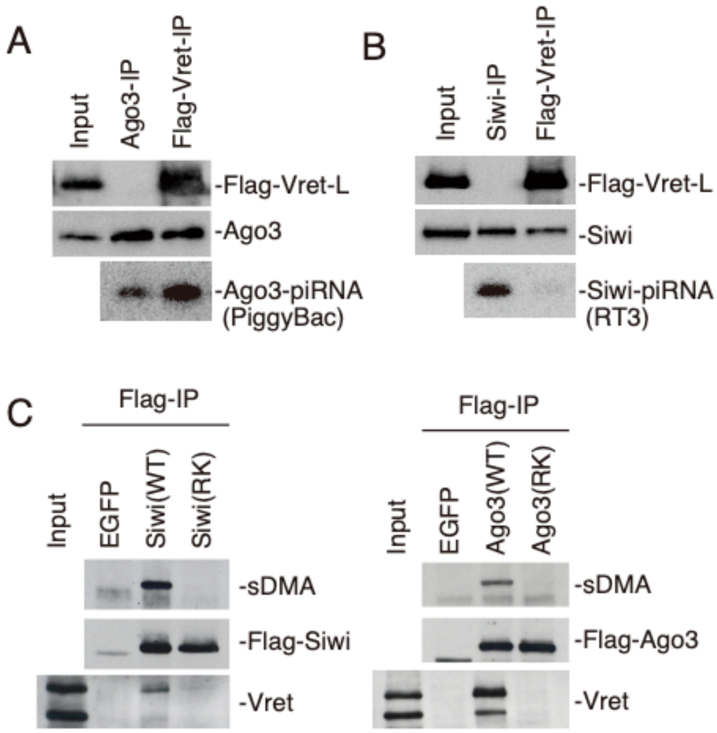


**Fig. 23. Vret associates with Ago3-piRISC and Apo-Siwi in sDMA dependent manner**

(A) Vret interacts with Ago3 in piRISC form. Northern blotting showing that PiggyBac-piRNA is abundantly loaded onto Ago3 associated with Vret. (B) Vret interacts with apo-Siwi. Northern blotting showing that RT3-piRNA is hardly loaded onto Siwi associated with Vret. (C) Immunoprecipitation and subsequent western blotting show that Siwi and Ago3 RK mutants, which are defective in sDMA modification, fail to co-purify with Vret.

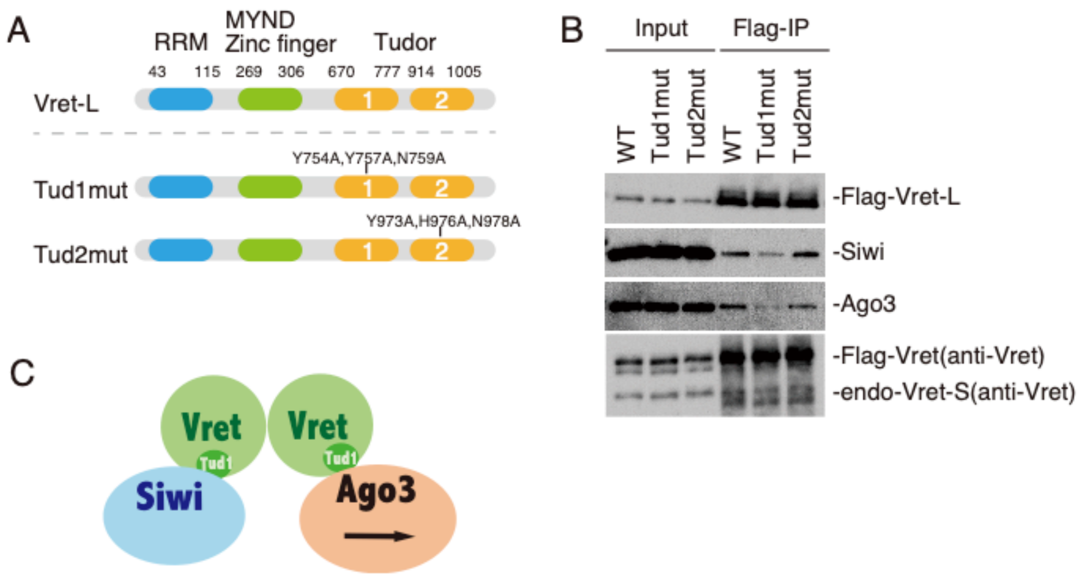


**Fig. 24. Vret interacts with Siwi and Ago3 through Tud1 domain**

(A) Domain structures of Tud mutant. Tyr754, Tyr757, Asn759 are mutated to alanine in Tud1 mutant and Tyr973, His976, Asn978 are mutated to alanine in Tud2 mutant. (B) Immunoprecipitation and subsequent western blotting show that Vret Tud1 mutant only weakly associates with Siwi and Ago3. Top: Western blotting with anti-Flag antibodies. Second from the top: Western blotting with anti-Siwi antibodies. Third from the top: Western blotting with anti-Siwi antibodies. Bottom: Western blotting with anti-Vret antibodies. (C) Model of Ago3-Vret-Siwi complex.

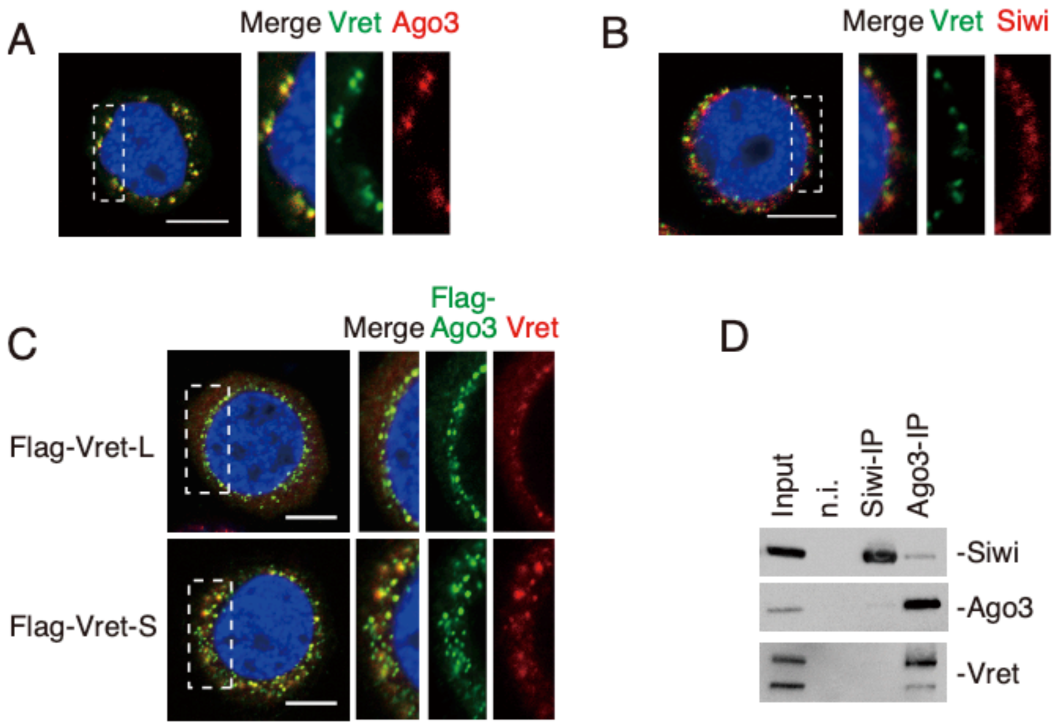


**Fig. 25. Vret localizes at Ago3-positive nuage**

(A) Immunostaining shows Vret completely co-localizes with Ago3 at nuage. (B) Immunostaining shows Vret partially co-localizes with Siwi at nuage. (C) Both exogenous Flag-Vret-L and -S co-localize with endogenous Ago3 at nuage. (D) Western blotting showing the presence of Siwi in the Ago3 complex.

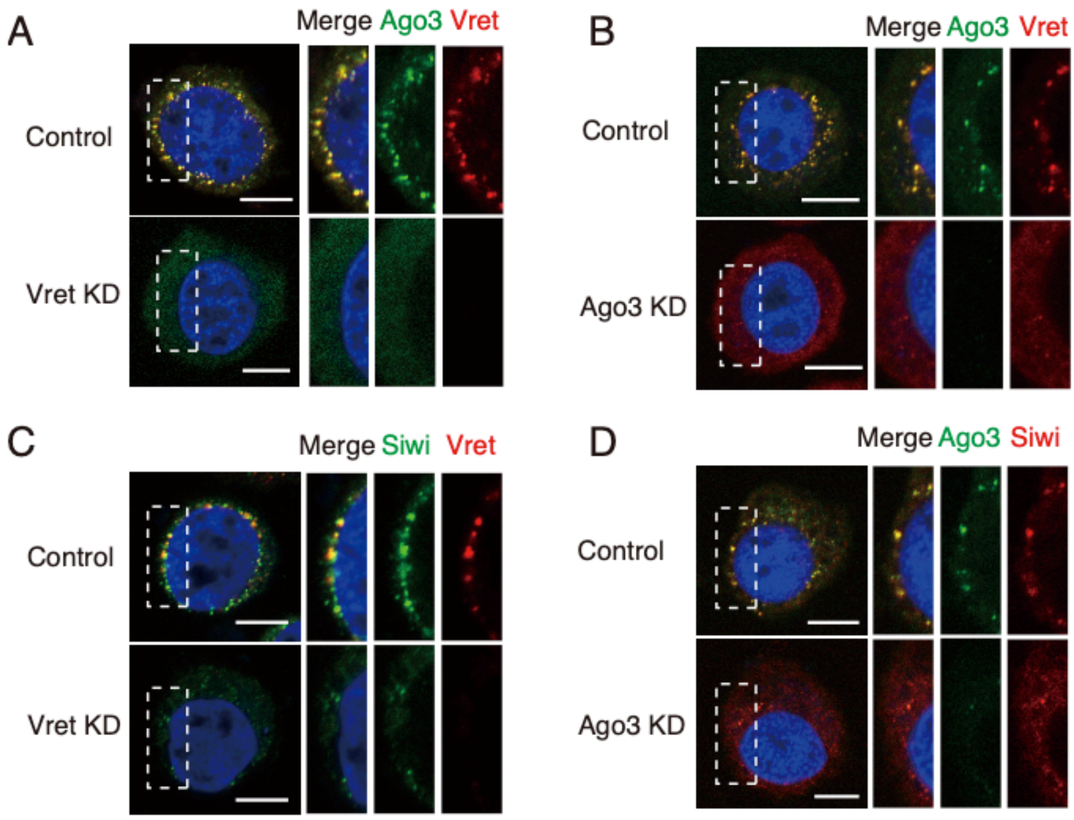


**Fig. 26. Depletion of Vret or Ago3 collapses Ago3-positive nuage formation**

(A) Immunofluorescence showing Ago3 signals in Vret-depleted BmN4 cells. (B) Immunofluorescence showing Vret signals in Ago3-depleted BmN4 cells. (C) Immunofluorescence showing Siwi signals in Vret-depleted BmN4 cells. (D) Immunofluorescence showing Siwi signals in Ago3-depleted BmN4 cells.

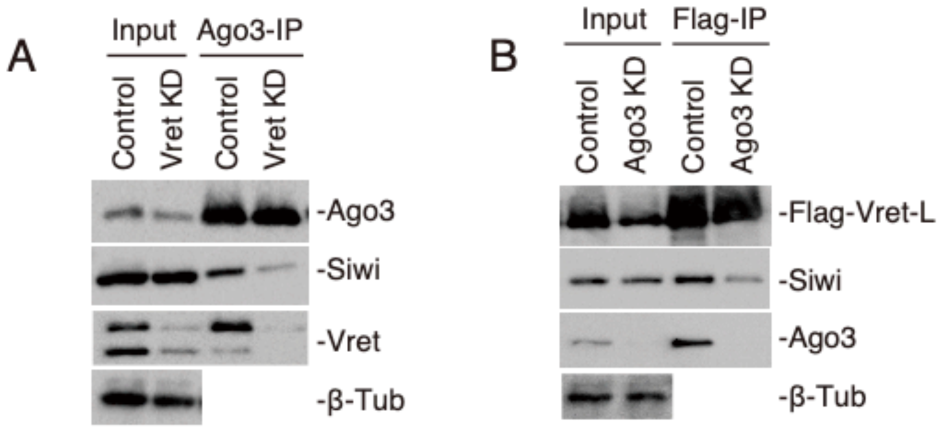


**Fig. 27. Knockdown of Vret or Ago3 collapses Ago3-Siwi interaction, Vret-Siwi interaction respectively.**

(A) Immunopreciapitation of Ago3 from Vret depleted cells shows weaker interaction between Ago3 and Siwi. (B) Immunopreciapitation of Flag-Vret-L from Ago3 depleted and Flag-Vret-L transfected cells shows weaker interaction between Flag-Vret-L and Siwi.

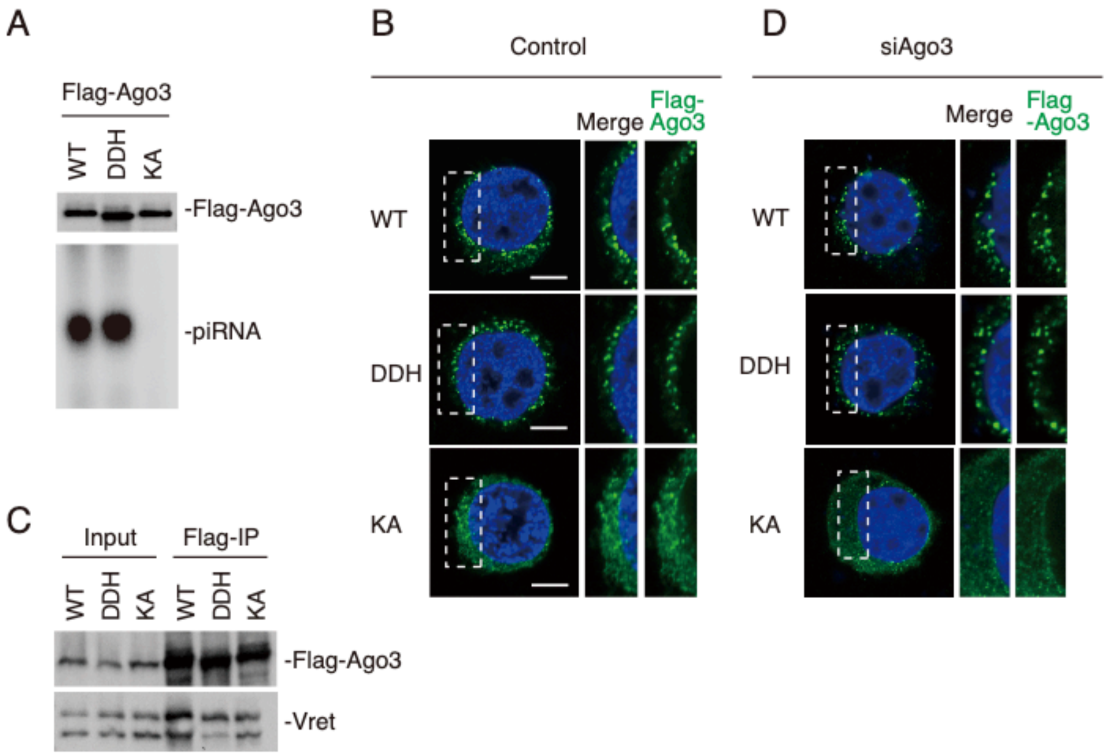


**Fig. 28. Target-binding capability is required for Ago3 to localized at nuage**

(A) $^{32}$P-labeling showing Flag-Ago3 DDH mutant, which is a catalytic dead mutant, normally associates with piRNAs as WT whereas KA mutant, whose Lys637 in MID domain is mutated to alanine hardly associates with. (B) Immunostaining of Flag-Ago3 WT, DDH mutant and KA mutant in normal condition. (C) Flag-Ago3 immunoprecipitations showing all mutants are able to interact with Vret. (D) Immunostaining of Flag-Ago3 WT, DDH mutant and KA mutant under Ago3-depleted condition.

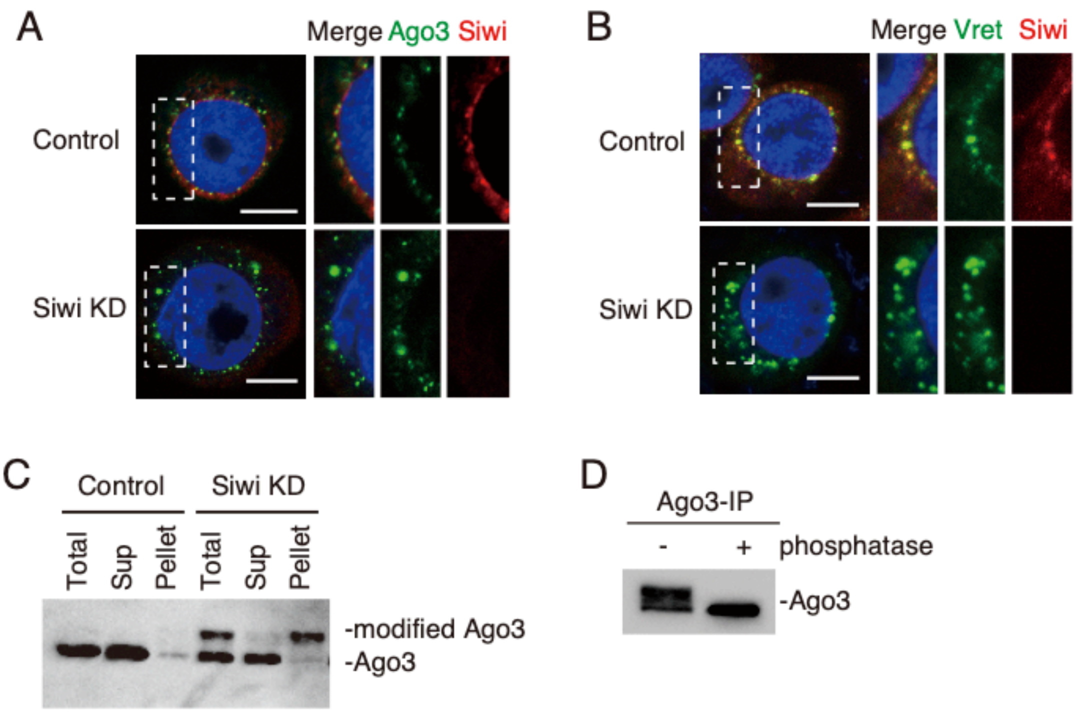


**Fig. 29. Knockdown of Siwi induces aggregation and phosphorylation of Ago3**

(A) Immunofluorescence showing Ago3 signals in Siwi-depleted BmN4 cells. Ago3 is aggregated at nuage. (B) Immunofluorescence showing Vret signals in Siwi-depleted BmN4 cells. Ago3 is aggregated at nuage. (C) Western blotting showing a half of Ago3 upon Siwi depletion migrated more slowly than Ago3 in normal cells. The slowly migrating Ago3 was detected in the pellet fraction while Ago3 in normal cells was detected in the supernatant fraction after centrifugation. (D) Western blotting shows that Ago3 appeared as a single band upon phosphatase treatment against immunoisolated Ago3.

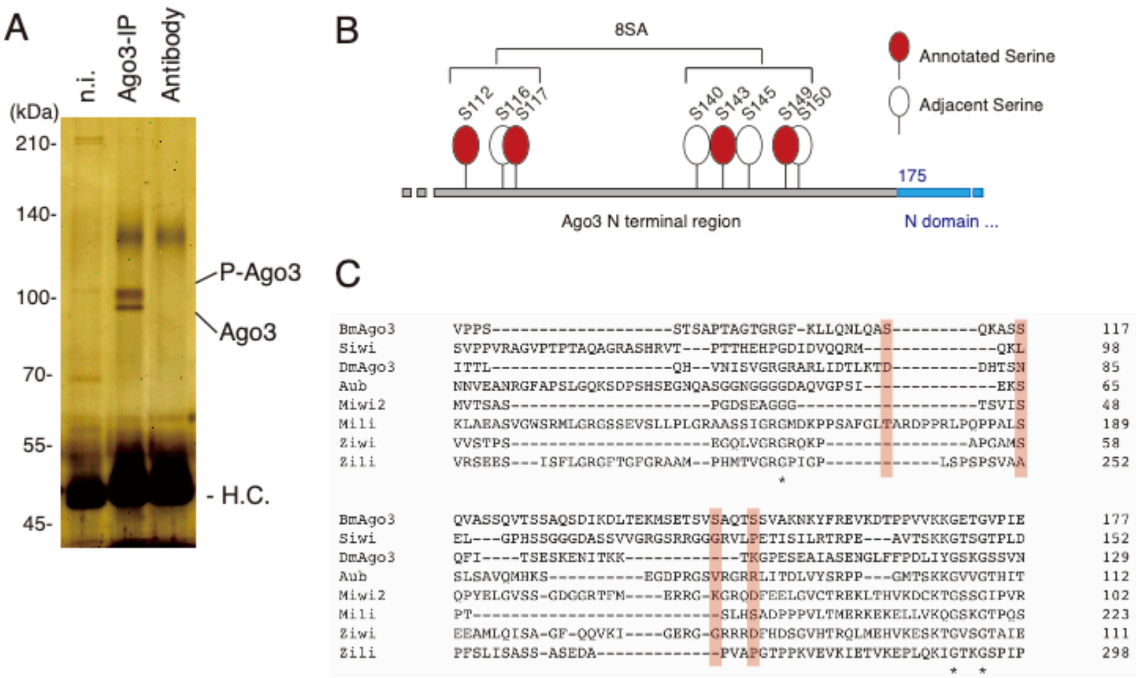


**Fig. 30. Mass spectrometry identifies four phosphorylated Serine residues.**

(A) Silver staining showing unphosphorylated and phosphorylated Ago3 immunoisolated from Siwi-depleted BmN4 cells. (B) Phosphorylation sites in P-Ago3. (C) Sequence alignment of N-terminal region of PIWI proteins in silkworm, fly, mice and zebrafish. Phosphorylated sites are highlighted in red.

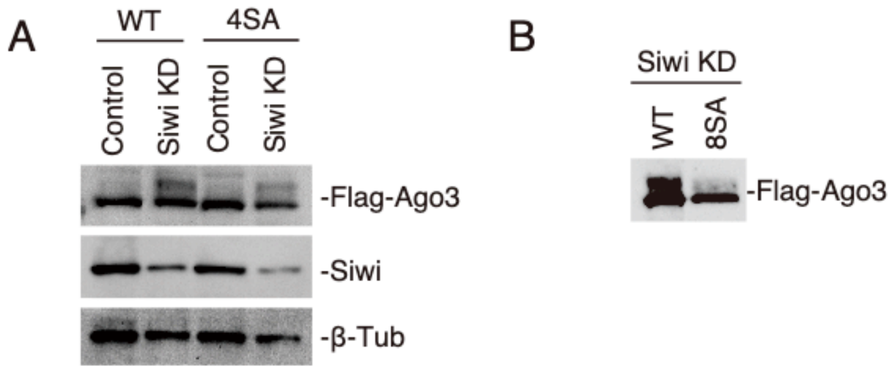


**Fig. 31. 8SA mutant is a phosphorylation-defective Ago3 mutant**

(A) Western blotting is conducted from Flag-Ago3 4SA mutant transfected and Siwi-depleted BmN4. 4SA mutant does not lose phosphorylation. (B) The Ago3 8SA mutant is no longer phosphorylated in BmN4 cells.

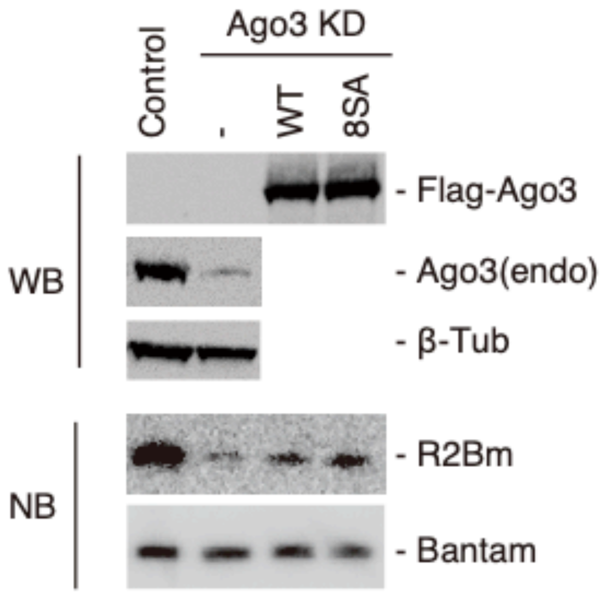


**Fig. 32. Phosphorylation of Ago3 is dispensable for Siwi-piRNA production**

The Ago3 8SA mutant restored the defects in piRNA production caused by loss of Ago3. Northern blotting (NB) was performed for visualizing R2Bm-piRNA. Bantam miRNA was detected as a control.

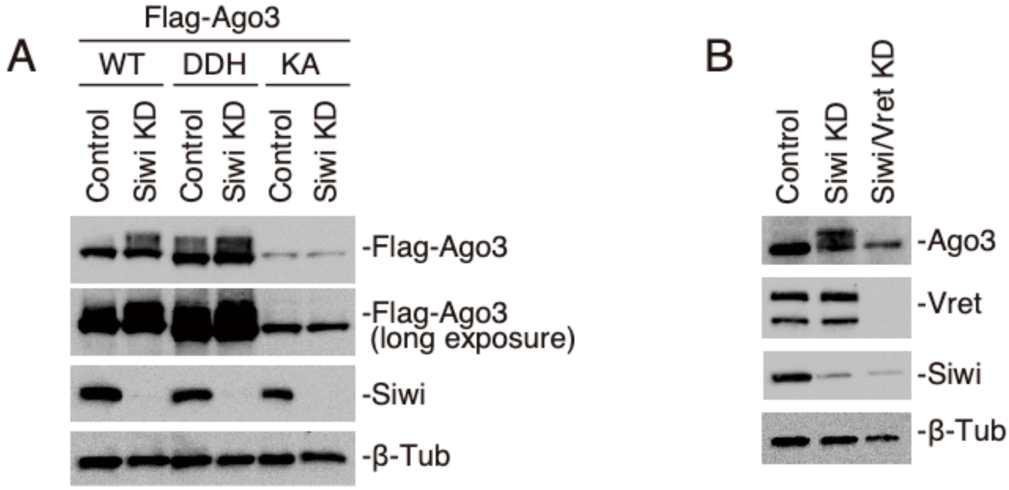


**Fig. 33. Ago3 gets phosphorylated after piRISC formation**

(A) The DDH mutant but not KA mutant was phosphorylated in Siwi-lacking BmN4 cells. DDH mutant is phosphorylated under normal condition. (B) Under Siwi/Vret double knockdown condition, Ago3 is not phosphorylated.

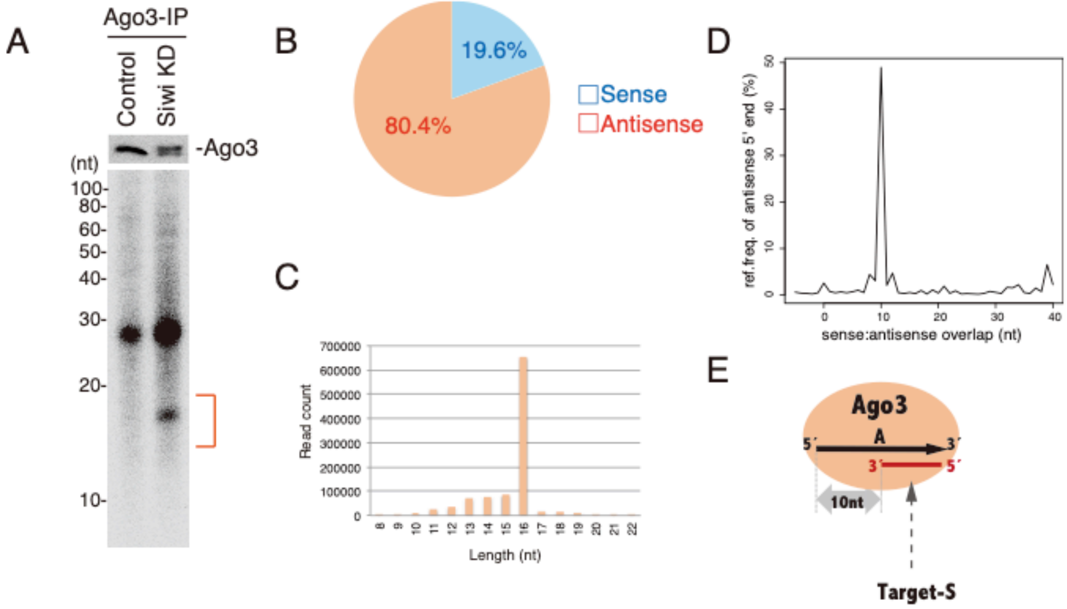


**Fig. 34. Target-Ss associate with Ago3 from Siwi-depleted cells**

(A) $^{32}$P-labeling of RNAs isolated from Ago3 (a mixture of unphosphorylated and phosphorylated shown in Fig. 30A) immunopurified from Siwi-depleted BmN4 cells. Short RNAs indicating with red bracket specifically associated with Ago3 from Siwi-depleted cells. (B) 80.4 % of 15-20 nt RNAs isolated from RNA gel in Fig. 34A corresponding transposon sequences are antisense to transposon mRNAs. Hereafter, I call the RNAs Target-Ss. (C) The size distribution of Target-Ss. (D) Examination of the distance between the 3´ end of Target-Ss and the 5´ end of Ago3-bound piRNAs. (E) Target-Ss are by-products of Ago3 cleavage.

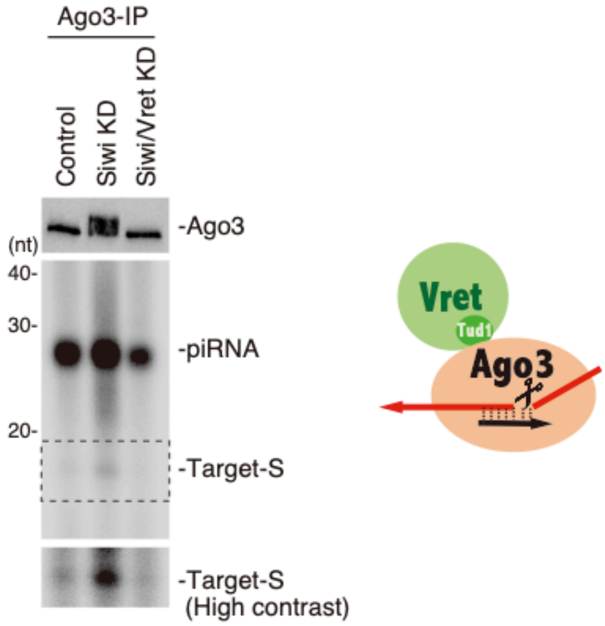


**Fig. 35. Ago3 does not associate with Target-Ss in Siwi/Vret double knockdown cells**

$^{32}$P-labeling of RNAs isolated from Ago3. Target-Ss are isolated from Siwi-depleted BmN4 but are not isolated from Siwi/Vret double knockdown cells.

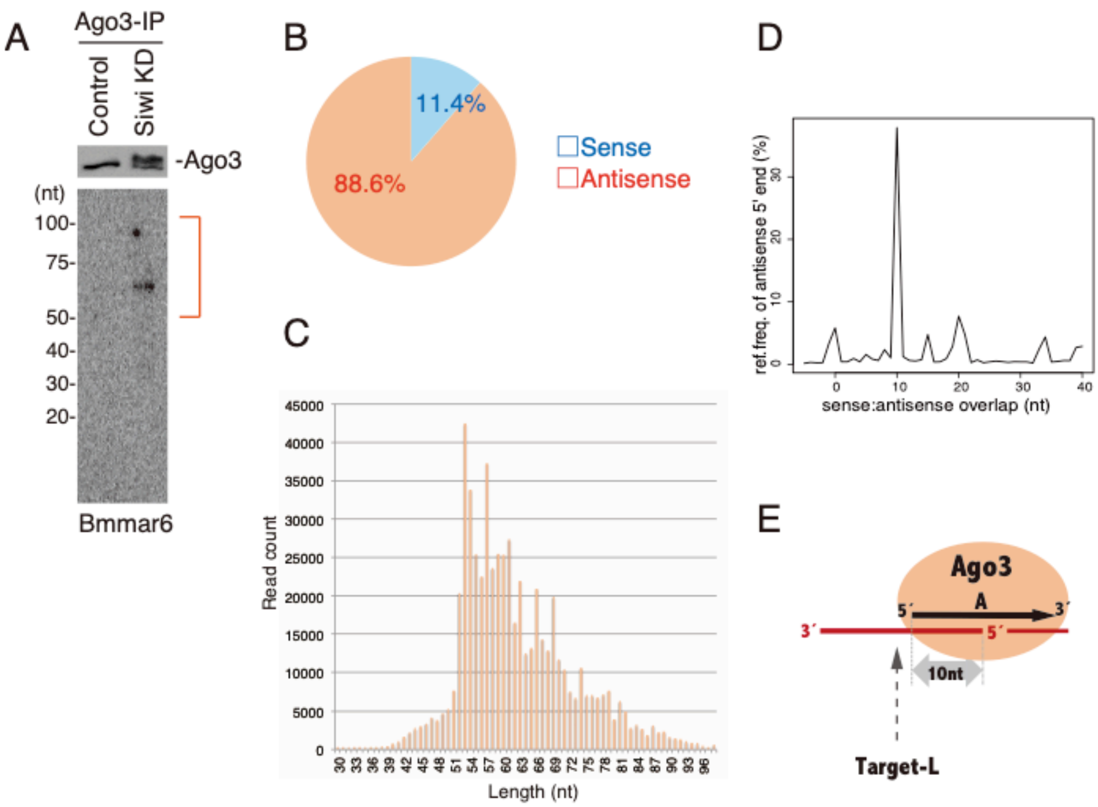


**Fig. 36. Target-Ls associate with Ago3 from Siwi-depleted cells**

(A) Northern blotting using a probe for Bmmar6-piRNA shows that the piRNA precursors are detected in the Ago3 complex. ~60nt RNAs indicating with red bracket specifically associated with Ago3 from Siwi-depleted cells. (B) 88.6 % of the transposon-derived piRNA precursors showing in Fig. 36A with red bracket are antisense to transposon mRNAs. Hereafter, I call the RNAs Target-Ls. (C) The size distribution of Target-Ls. (D) Examination of the distance between the 5′ end of Target-Ls and the 5′ end of Ago3-bound piRNAs. (E) Target-Ls are supposed to be Siwi-piRNA intermediates.

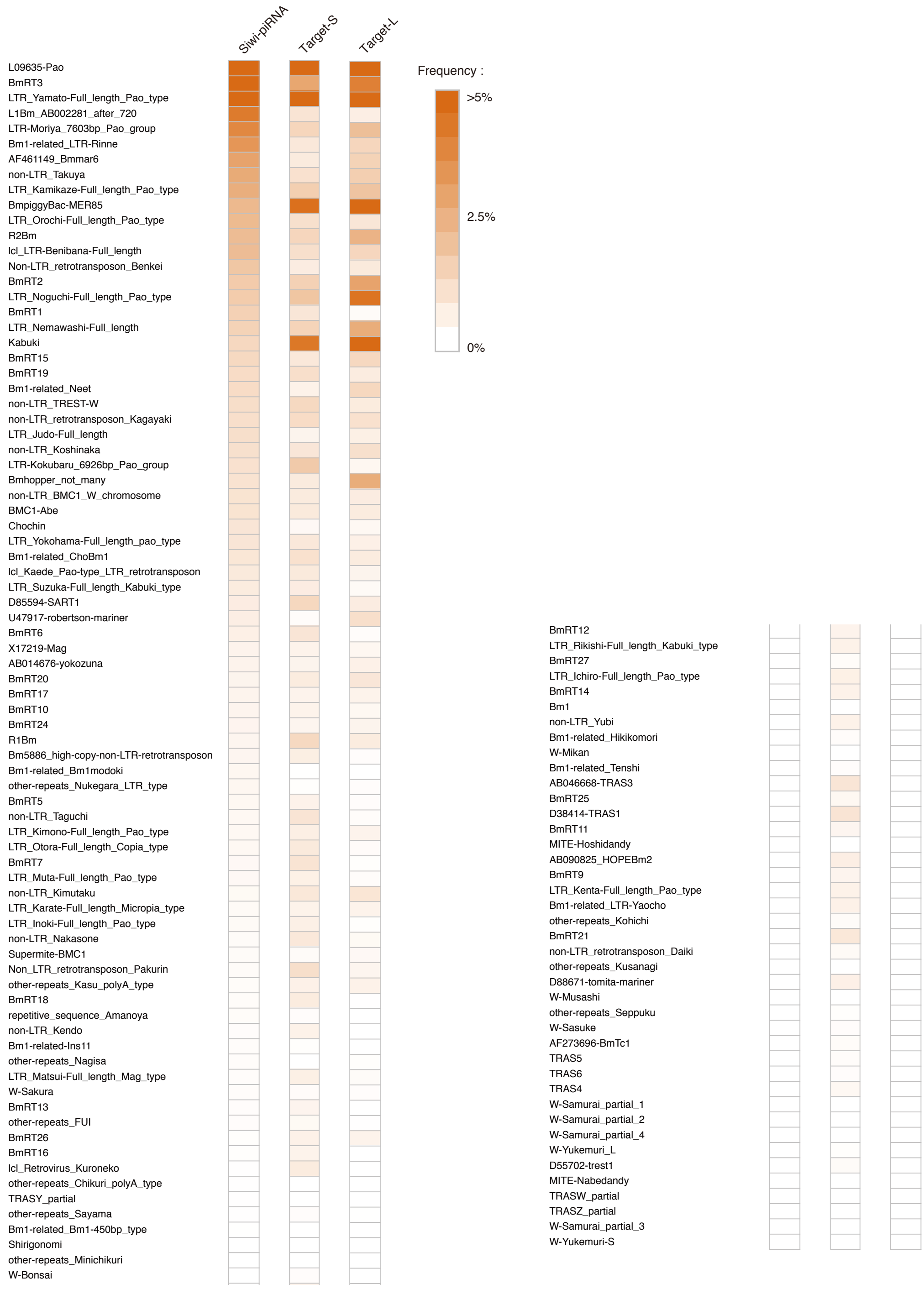


## Fig. 37. Target-S and -L are derived from variety of transposons

Heat maps show read frequency of transposon derived Ago3-piRNA, Target-S and -L. Color intensities indicate the degree of read frequency: (orange) higher; (white) lower.

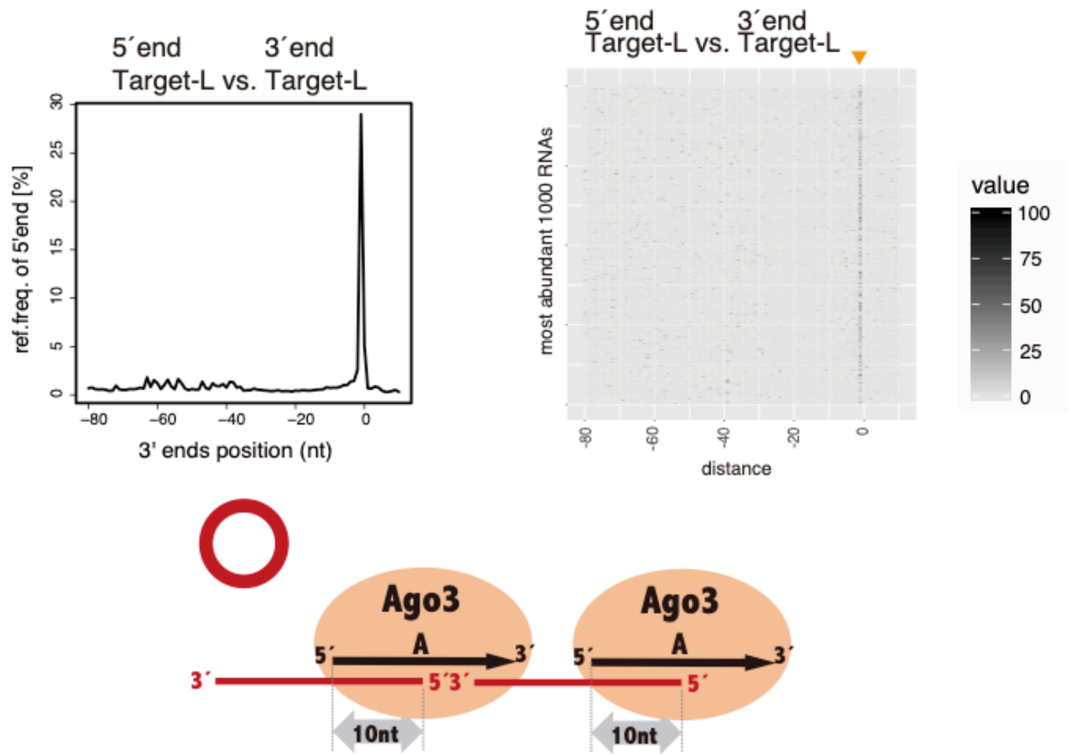


**Fig. 38. Target-Ls are yielded tandem**

Left panel shows Target-Ls are produced tandem. Right panel shows most abundant 1000 reads of Target-Ls are produced tandem.

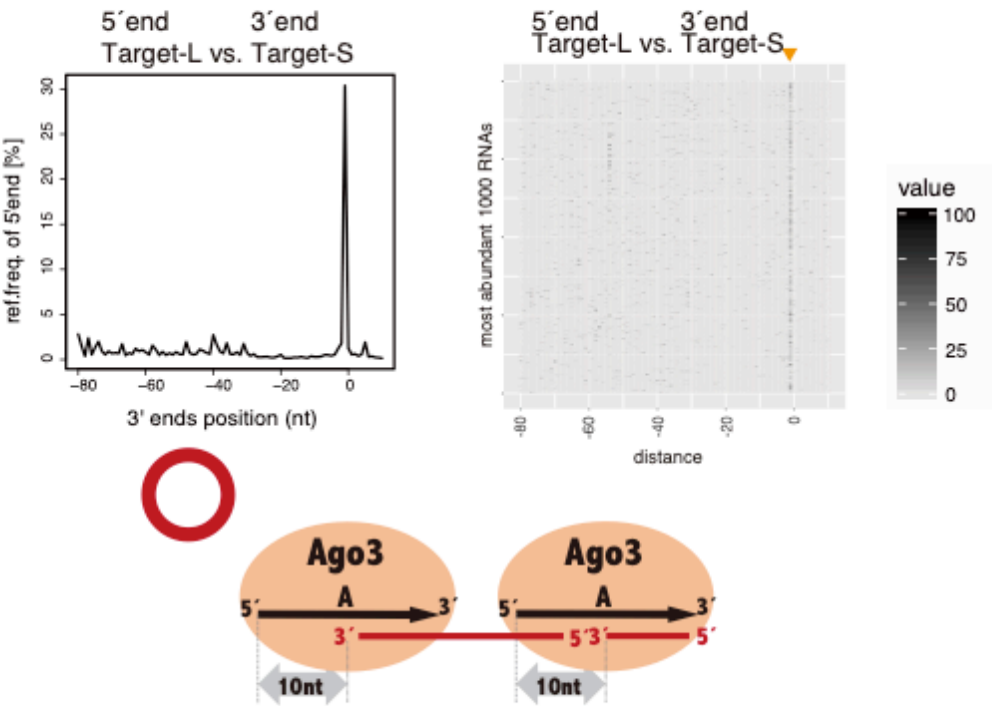


**Fig. 39. Target-Ss are yielded 1nt downstream of Target-Ls**

Left panel shows Target-Ls are produced 1nt downstream of 3´ ends of Target-Ss. Right panel shows Most abundant 1000 reads of Target-Ls are produced 1nt downstream of 3´ ends of Target-Ss.

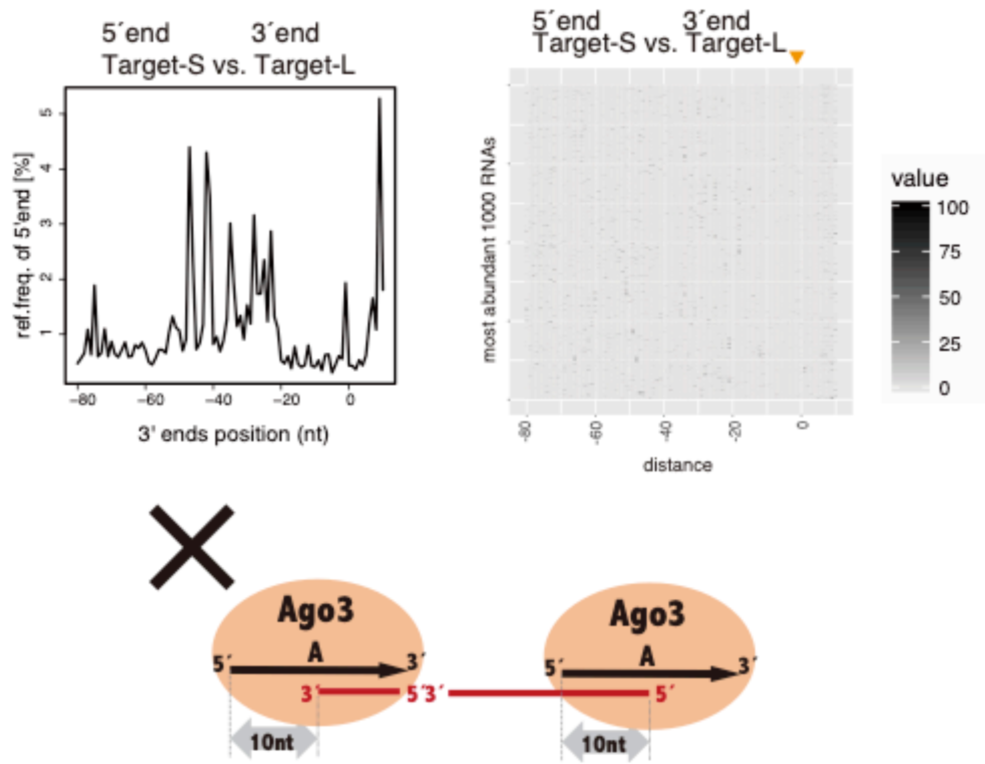


**Fig. 40. Target-Ls are not yielded 1nt downstream of Target-Ss**

Left panel shows Target-Ss are not produced 1nt downstream of 3´ ends of Target-Ls. Right panel shows Most abundant 1000 reads of Target-Ss are produced 1nt downstream of 3´ ends of Target-Ls.

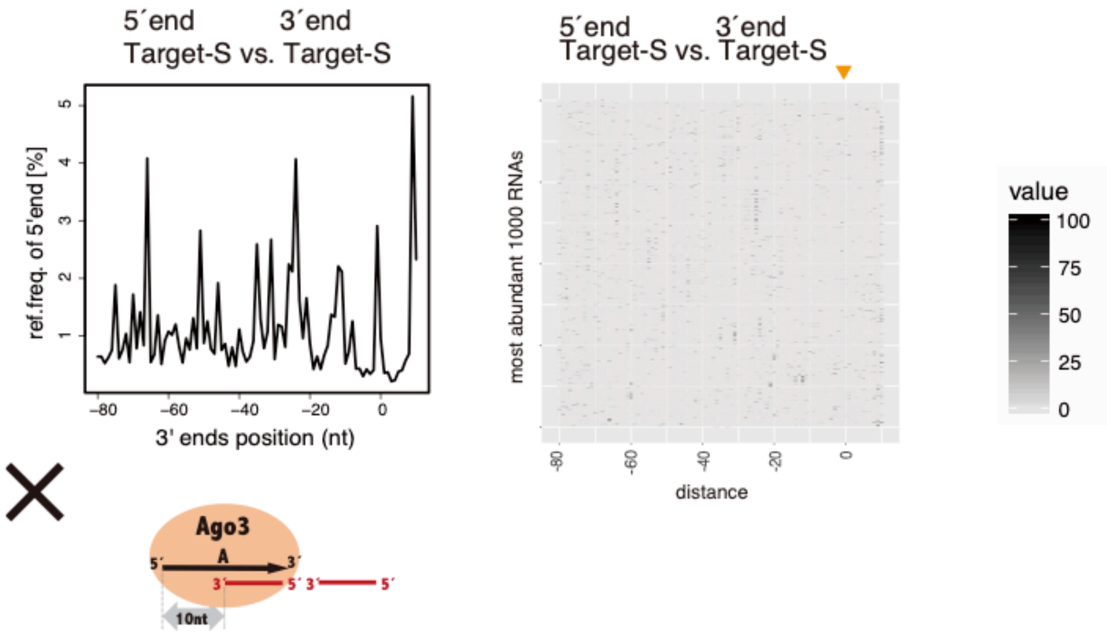


**Fig. 41. Target-Ss are not yielded tandem**

Left panel shows Target-Ss are not produced tandem. Right panel shows most abundant 1000 reads of Target-Ss are not produced tandem.

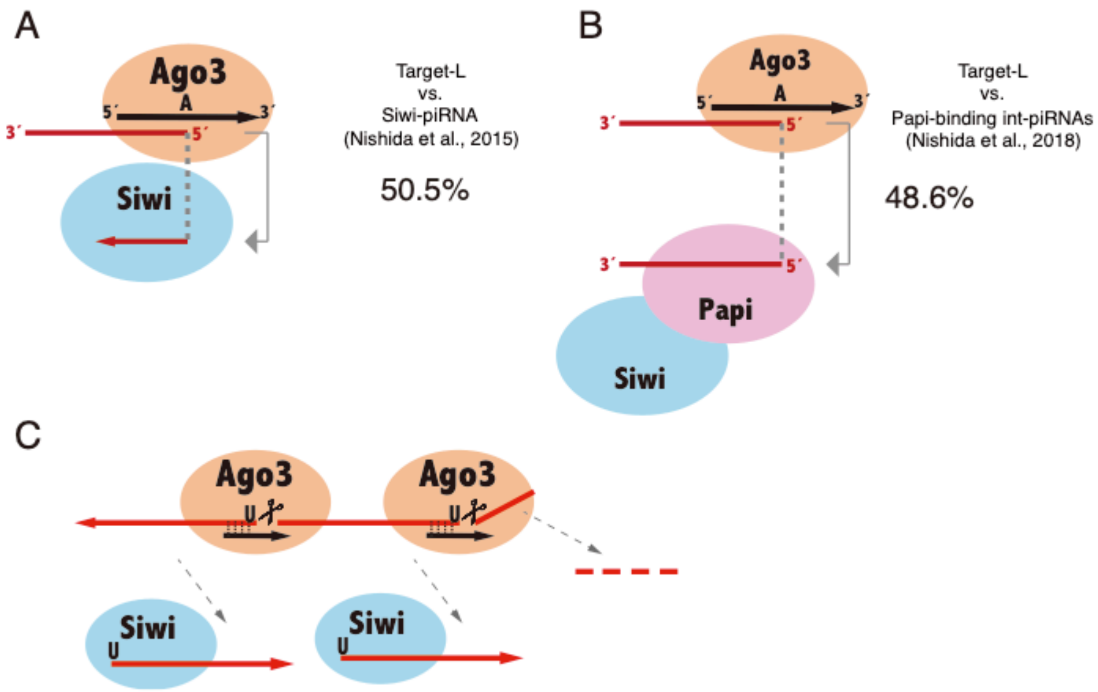


**Fig. 42. Target-Ls are utilized as Siwi-piRNA intermediates**

(A) 50.5% of Target-Ls share their 5´ ends with Siwi-piRNAs (Nishida et al., 2015). (B) 48.6% of Target-Ls share their 5´ ends with Papi-binding RNAs (Nishida et al., 2018). (C) Model of successive Siwi-piRNA intermediate production by Ago3-piRISCs.

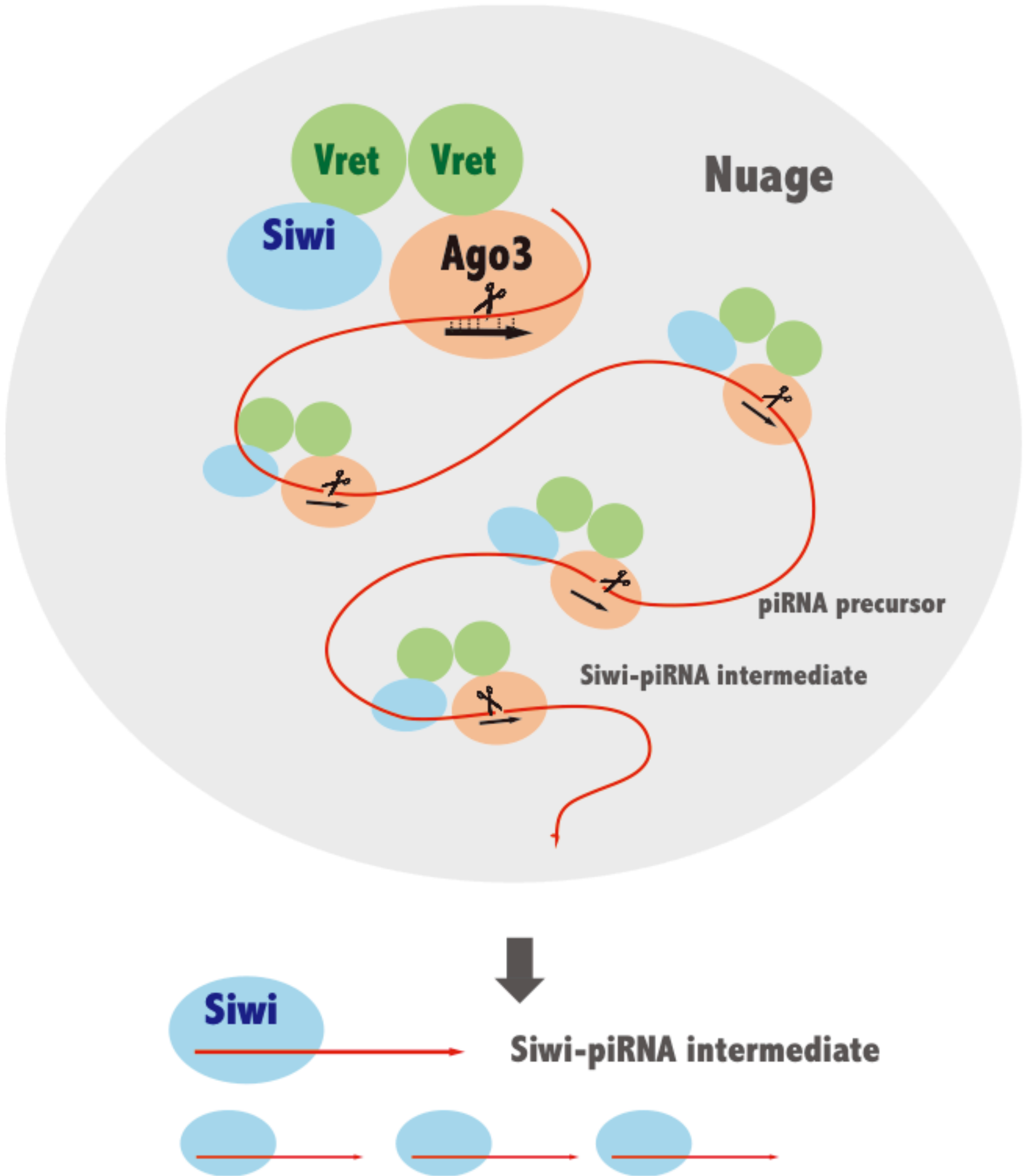


**Fig. 43. Model of Ago3-dependent Siwi-piRNA production**

# 4. Discussion

## 4. Discussion

Through my researches documented above, I elucidate molecular mechanism of two different antisense piRNA biogenesis pathways. Then I propose a new model for piRNA biogenesis in silkworm germ cells (Fig. 44). In primary pathway, Siwi-piRNA intermediates are maturated by Zuc in Papi complex. Cleavage positions are determined by 5´ end protection by Siwi but not Zuc itself. In ping-pong cycle, Siwi-piRNA intermediates are produced successively by Ago3-piRISCs anchored at nuage by Vret. Vret associates with Apo-Siwi and Ago3-piRISC through sDMA-tudor domain interaction. Assembly Siwi-Vret-Ago3 complex is necessary for Siwi-piRNA intermediates production by Ago3.

Previous research showed Trim processed 3´ end of piRNAs (Izumi et al., 2016) but the amount of piRNA was not changed by Trim depletion in contrast of Zuc depletion in my study. Then I concluded dominant nuclease for 3´ end formation of piRNA is Zuc. However, depletion of Trim induced extention of 3´ end of piRNAs and part of the cleavage products by Zuc *in vitro* are a few nt longer than endogenous Siwi-piRNAs indeed. These results suggest Trim play a role for 3´ end formation as fine-tuner. Zuc cleaved 3´ ends of Siwi-piRNA intermediates firstly. When the length of cleaved RNA is mature piRNA size, the 3´ end is accommodated in 3´ binding pocket in PAZ domain. When cleaved RNA is longer than mature piRNA, Trim trims 3´ end and mature piRNA is generated. The range of length of *Bombyx* piRNA is 23-30nt but 27-28nt piRNAs are apparently abundant (Nishida et al., 2015). I imagine combinational function of Zuc and Trim, endonuclease and exonuclease in other word, converges the length of piRNA.

Vret associates with Apo-Siwi and Ago3-piRISC dependent on sDMA modification and Ago3-Vret-Siwi complex seems to be indispensable for Ago3-dependent Siwi-piRNA production. Then one question, how Vret recognizes Apo-Siwi and Ago3-piRISC respectively, arises. For Ago3-dependent piRNA production, Ago3-piRISC-Vret-Apo-Siwi combination is only meaningful. For example, Apo-Ago3-Vret-Siwi-piRISC or Ago3-piRISC-Vret-Ago3-piRISC is meaningless. Therefore, the complex formation needs to be highly regulated. To accomplish to make correct complex, Vret is require to overcome two difficulties. First, Vret has to distinguish Siwi and Ago3. Second Vret has to recognize piRISC form or Apo form. *In vitro* binding assays using recombinant Vret and mutant PIWI proteins disable to be piRISCs are helpful to elucidate the molecular mechanism. In the future, I would like to prepare them and calculate the efficacy of PIWI-Vret interaction quantitatively. Moreover, collaboration with structural biologist is going to be effective breakthrough. If structure of Ago3-Vret-Siwi complex is uncovered, it would give me direct answer for the question how Vret recognize Apo-Siwi and Ago3-piRISC respectively.

There is another interesting point on PIWI's sDMA-Tudor domain interaction. Both Papi and Vret associated with Apo-Siwi dependent on sDMA modification. Since the former localizes at mitochondrion but the latter localizes at nuage, some proteins are required to distribute Apo-Siwi to mitochondrion and nuage appropriately. However such proteins have not been identified. My research and previous researches suggest mitochondrion is place for maturation of Siwi-piRNA whereas nuage is room for piRNA intermediates production. Different processing phases held at different organelles are unique feature of piRNA biogenesis. Thus, mechanism of transportation of Apo-Siwis will be interesting theme.

The last piece in ping-pong cycle, which has not been identified yet, is Vasa-like helicase removing cleavage products from Ago3-piRISCs and loading them onto Siwi (Fig. 44). Second half of ping-pong cycle has been difficult to research because primary pathway compensates Siwi-piRNA when Ago3-dependent Siwi-piRNA biogenesis pathway is disrupted. Since the amount of Siwi-piRNA is only slightly reduced by knockdown of Ago3, some other evaluation method was needed for research of second half of ping-pong cycle. I show that northern blotting using probes against Ago3 dependent Siwi-piRNAs is able to evaluate whether some factors play a role for second half of ping-pong cycle in this research. I think this method open the door to perform knockdown screening for the Vasa-like helicase. I also identified Vret as co-factor of Ago3 to produce Siwi-piRNA intermediates and the Vasa-like helicase should be involved in Vret-Ago3 complex. Therefore, MS analysis for co-immunoprecipitates of Vret would be helpful to list candidate helicases.

There still remain many mysteries in piRNA biogenesis as written here. I hope my research will be clue to uncover the molecular mechanism of ping-pong cycle

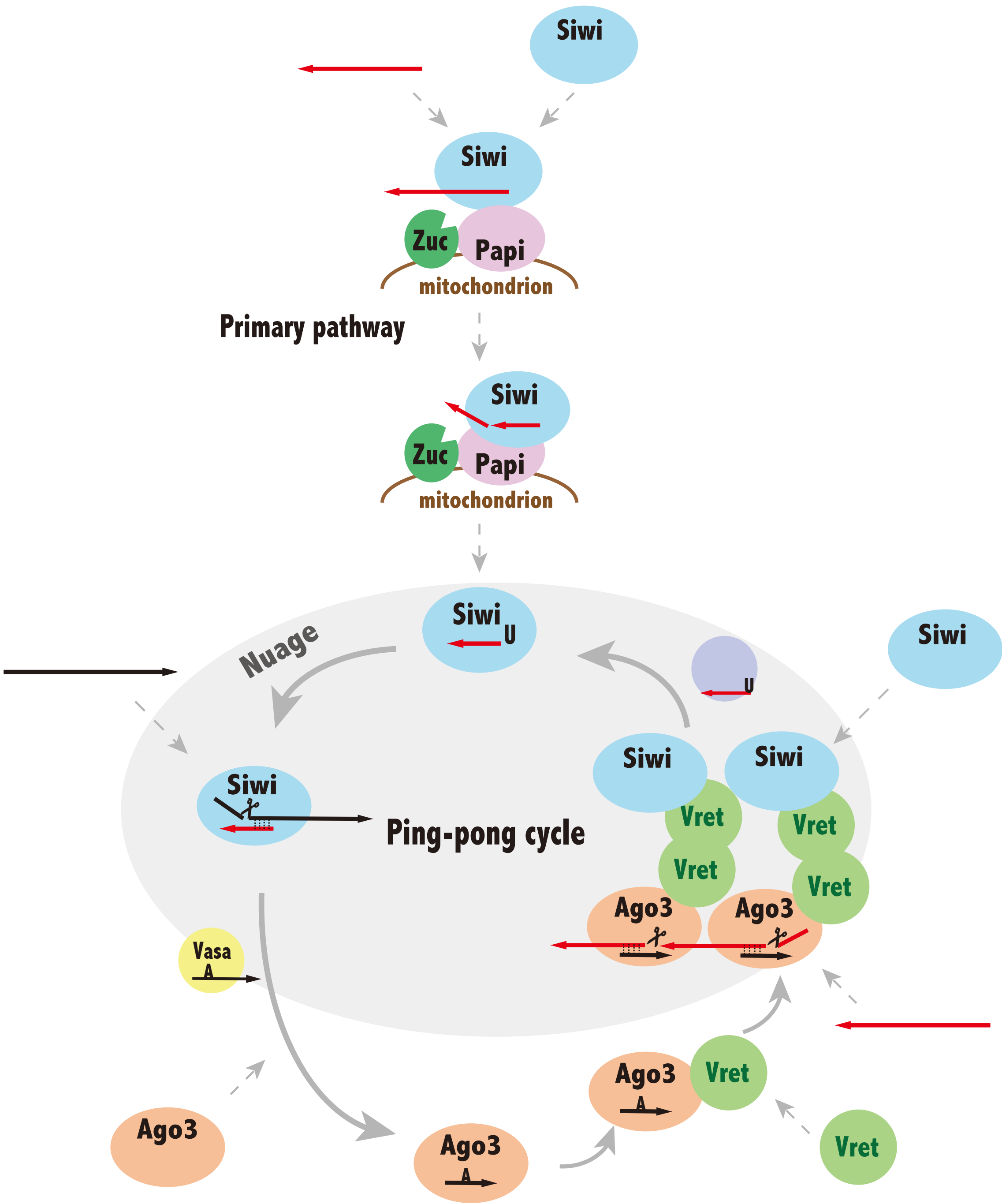


**Fig. 44. Two different pathways for piRNA biogenesis in BmN4**

# 5. References

## 5. References


al-Mukhtar, K.A., and Webb, A.C. (1971). An ultrastructural study of primordial germ cells, oogonia and early oocytes in Xenopus laevis. J. Embryol. Exp. Morphol. *26*, 195–217.

Aravin, A.A., Lagos-Quintana, M., Yalcin, A., Zavolan, M., Marks, D., Snyder, B., Gaasterland, T., Meyer, J., and Tuschl, T. (2003). The small RNA profile during Drosophila melanogaster development. Dev. Cell *5*, 337–350.

Batista, P.J., Ruby, J.G., Claycomb, J.M., Chiang, R., Fahlgren, N., Kasschau, K.D., Chaves, D.A., Gu, W., Vasale, J.J., Duan, S., et al. (2008). PRG-1 and 21U-RNAs interact to form the piRNA complex required for fertility in C. elegans. Mol. Cell *31*, 67–78.

Beausoleil, S.A., Villén, J., Gerber, S.A., Rush, J., and Gygi, S.P. (2006). A probability-based approach for high-throughput protein phosphorylation analysis and site localization. Nat. Biotechnol. *24*, 1285–1292.

Brennecke, J., Aravin, A.A., Stark, A., Dus, M., Kellis, M., Sachidanandam, R., and Hannon, G.J. (2007). Discrete small RNA-generating loci as master regulators of transposon activity in Drosophila. Cell *128*, 1089–1103.

Czech, B., Preall, J.B., McGinn, J., and Hannon, G.J. (2013). A transcriptome-wide RNAi screen in the Drosophila ovary reveals factors of the germline piRNA pathway. Mol. Cell *50*, 749–761.

Eddy, E.M. (1975). Germ plasm and the differentiation of the germ cell line. Int. Rev. Cytol. *43*, 229–280.

Ghildiyal, M., and Zamore, P.D. (2009). Small silencing RNAs: an expanding universe. Nat. Rev. Genet. *10*, 94–108.

Girard, A., Sachidanandam, R., Hannon, G.J., and Carmell, M.A. (2006). A germline-specific class of small RNAs binds mammalian Piwi proteins. Nature *442*, 199–202.

Grimson, A., Srivastava, M., Fahey, B., Woodcroft, B.J., Chiang, H.R., King, N., Degnan, B.M., Rokhsar, D.S., and Bartel, D.P. (2008). Early origins and evolution of microRNAs and Piwi-interacting RNAs in animals. Nature *455*, 1193–1197.

Gunawardane, L.S., Saito, K., Nishida, K.M., Miyoshi, K., Kawamura, Y., Nagami, T., Siomi, H., and Siomi, M.C. (2007). A slicer-mediated mechanism for repeat-associated siRNA 5' end formation in Drosophila. Science *315*, 1587–1590.

Han, B.W., Wang, W., Li, C., Weng, Z., and Zamore, P.D. (2015). Noncoding RNA. piRNA-guided transposon cleavage initiates Zucchini-dependent, phased piRNA production. Science *348*, 817–821.

Handler, D., Olivieri, D., Novatchkova, M., Gruber, F.S., Meixner, K., Mechtler, K., Stark, A., Sachidanandam, R., and Brennecke, J. (2011). A systematic analysis of Drosophila TUDOR domain-containing proteins identifies Vreteno and the Tdrd12 family as essential primary piRNA pathway factors. EMBO J. *30*, 3977–3993.

Handler, D., Meixner, K., Pizka, M., Lauss, K., Schmied, C., Gruber, F.S., and Brennecke, J. (2013). The Genetic Makeup of the Drosophila piRNA Pathway. Mol. Cell *50*, 762–777.

Hayashi, R., Schnabl, J., Handler, D., Mohn, F., Ameres, S.L., and Brennecke, J. (2016). Genetic and mechanistic diversity of piRNA 3'-end formation. Nature *539*, 588–592.

Hirano, T., Iwasaki, Y.W., Lin, Z.Y.-C., Imamura, M., Seki, N.M., Sasaki, E., Saito, K., Okano, H., Siomi, M.C., and Siomi, H. (2014). Small RNA profiling and characterization of piRNA clusters in the adult testes of the common marmoset, a model primate. RNA *20*, 1223–1237.

Honda, S., Kirino, Y., Maragkakis, M., Alexiou, P., Ohtaki, A., Murali, R., Mourelatos, Z., and Kirino, Y. (2013). Mitochondrial protein BmPAPI modulates the length of mature piRNAs. RNA *19*, 1405–1418.

Houwing, S., Kamminga, L.M., Berezikov, E., Cronembold, D., Girard, A., van den Elst, H., Filippov, D. V., Blaser, H., Raz, E., Moens, C.B., et al. (2007). A Role for Piwi and piRNAs in Germ Cell Maintenance and Transposon Silencing in Zebrafish. Cell *129*, 69–82.

Huang, H.-Y., Houwing, S., Kaaij, L.J.T., Meppelink, A., Redl, S., Gauci, S., Vos, H., Draper, B.W., Moens, C.B., Burgering, B.M., et al. (2011). Tdrd1 acts as a molecular scaffold for Piwi proteins and piRNA targets in zebrafish. EMBO J. *30*, 3298–3308.

Ipsaro, J.J., Haase, A.D., Knott, S.R., Joshua-Tor, L., and Hannon, G.J. (2012). The structural biochemistry of Zucchini implicates it as a nuclease in piRNA biogenesis. Nature *491*, 279–283.

Izumi, N., Shoji, K., Sakaguchi, Y., Honda, S., Kirino, Y., Suzuki, T., Katsuma, S., and Tomari, Y. (2016). Identification and Functional Analysis of the Pre-piRNA 3' Trimmer in Silkworms. Cell *164*, 962–973.

Jaskiewicz, L., Bilen, B., Hausser, J., and Zavolan, M. (2012). Argonaute CLIP--a method to identify in vivo targets of miRNAs. Methods *58*, 106–112.

Kawaoka, S., Minami, K., Katsuma, S., Mita, K., and Shimada, T. (2008a). Developmentally synchronized expression of two Bombyx mori Piwi subfamily genes, SIWI and BmAGO3 in germ-line cells. Biochem. Biophys. Res. Commun. *367*, 755–760.

Kawaoka, S., Hayashi, N., Katsuma, S., Kishino, H., Kohara, Y., Mita, K., and Shimada, T. (2008b). Bombyx small RNAs: genomic defense system against transposons in the silkworm, Bombyx mori. Insect Biochem. Mol. Biol. *38*, 1058–1065.

Kirino, Y., Kim, N., de Planell-Saguer, M., Khandros, E., Chiorean, S., Klein, P.S., Rigoutsos, I., Jongens, T.A., and Mourelatos, Z. (2009). Arginine methylation of Piwi proteins catalysed by dPRMT5 is required for Ago3 and Aub stability. Nat. Cell Biol. *11*, 652–658.

Klenov, M.S., Lavrov, S.A., Stolyarenko, A.D., Ryazansky, S.S., Aravin, A.A., Tuschl, T., and Gvozdev, V.A. (2007). Repeat-associated siRNAs cause chromatin silencing of retrotransposons in the Drosophila melanogaster germline. Nucleic Acids Res. *35*, 5430–5438.

Lau, N.C., Seto, A.G., Kim, J., Kuramochi-Miyagawa, S., Nakano, T., Bartel, D.P., and Kingston, R.E. (2006). Characterization of the piRNA Complex from Rat Testes. Science (80-. ). *313*, 363–367.

Li, C., Vagin, V. V, Lee, S., Xu, J., Ma, S., Xi, H., Seitz, H., Horwich, M.D., Syrzycka, M., Honda, B.M., et al. (2009). Collapse of germline piRNAs in the absence of Argonaute3 reveals somatic piRNAs in flies. Cell *137*, 509–521.

Lim, A.K., and Kai, T. (2007). Unique germ-line organelle, nuage, functions to repress selfish genetic elements in Drosophila melanogaster. Proc. Natl. Acad. Sci. *104*, 6714–6719.

Lim, R.S.M., Anand, A., Nishimiya-Fujisawa, C., Kobayashi, S., and Kai, T. (2014). Analysis of Hydra PIWI proteins and piRNAs uncover early evolutionary origins of the piRNA pathway. Dev. Biol. *386*, 237–251.

Liu, H., Wang, J.-Y.S., Huang, Y., Li, Z., Gong, W., Lehmann, R., and Xu, R.-M. (2010). Structural basis for methylarginine-dependent recognition of Aubergine by Tudor. Genes Dev. *24*, 1876–1881.

Liu, L., Qi, H., Wang, J., and Lin, H. (2011). PAPI, a novel TUDOR-domain protein, complexes with AGO3, ME31B and TRAL in the nuage to silence transposition. Development *138*, 1863–1873.

Malone, C.D., and Hannon, G.J. (2009). Small RNAs as Guardians of the Genome. Cell *136*, 656–668.

Malone, C.D., Brennecke, J., Dus, M., Stark, A., McCombie, W.R., Sachidanandam, R., and Hannon, G.J. (2009). Specialized piRNA pathways act in germline and somatic tissues of the Drosophila ovary. Cell *137*, 522–535.

Matsumoto, N., Nishimasu, H., Sakakibara, K., Nishida, K.M., Hirano, T., Ishitani, R., Siomi, H., Siomi, M.C., and Nureki, O. (2016). Crystal Structure of Silkworm PIWI-Clade Argonaute Siwi Bound to piRNA. Cell *167*, 484-497.e9.

Mohn, F., Handler, D., and Brennecke, J. (2015). Noncoding RNA. piRNA-guided slicing specifies transcripts for Zucchini-dependent, phased piRNA biogenesis. Science *348*, 812–817.

Munafò, M., Manelli, V., Falconio, F.A., Sawle, A., Kneuss, E., Eastwood, E.L., Seah, J.W.E., Czech, B., and Hannon, G.J. (2019). Daedalus and Gasz recruit Armitage to mitochondria, bringing piRNA precursors to the biogenesis machinery. Genes Dev. *33*, 844–856.

Nishida, K.M., Okada, T.N., Kawamura, T., Mituyama, T., Kawamura, Y., Inagaki, S., Huang, H., Chen, D., Kodama, T., Siomi, H., et al. (2009). Functional involvement of Tudor and dPRMT5 in the piRNA processing pathway in Drosophila germlines. EMBO J. *28*, 3820–3831.

Nishida, K.M., Iwasaki, Y.W., Murota, Y., Nagao, A., Mannen, T., Kato, Y., Siomi, H., and Siomi, M.C. (2015). Respective functions of two distinct Siwi complexes assembled during PIWI-interacting RNA biogenesis in Bombyx germ cells. Cell Rep. *10*, 193–203.

Nishida, K.M., Sakakibara, K., Iwasaki, Y.W., Yamada, H., Murakami, R., Murota, Y., Kawamura, T., Kodama, T., Siomi, H., and Siomi, M.C. (2018). Hierarchical roles of mitochondrial Papi and Zucchini in Bombyx germline piRNA biogenesis. Nature *555*, 260–264.

Nishimasu, H., Ishizu, H., Saito, K., Fukuhara, S., Kamatani, M.K., Bonnefond, L., Matsumoto, N., Nishizawa, T., Nakanaga, K., Aoki, J., et al. (2012). Structure and function of Zucchini endoribonuclease in piRNA biogenesis. Nature *491*, 284–287.

Pall, G.S., and Hamilton, A.J. (2008). Improved northern blot method for enhanced detection of small RNA. Nat. Protoc. *3*, 1077–1084.

Reuter, M., Chuma, S., Tanaka, T., Franz, T., Stark, A., and Pillai, R.S. (2009). Loss of the Mili-interacting Tudor domain–containing protein-1 activates transposons and alters the Mili-associated small RNA profile. Nat. Struct. Mol. Biol. *16*, 639–646.

Robine, N., Lau, N.C., Balla, S., Jin, Z., Okamura, K., Kuramochi-Miyagawa, S., Blower, M.D., and Lai, E.C. (2009). A broadly conserved pathway generates 3'UTR-directed primary piRNAs. Curr. Biol. *19*, 2066–2076.

Saito, K., Nishida, K.M., Mori, T., Kawamura, Y., Miyoshi, K., Nagami, T., Siomi, H., and Siomi, M.C. (2006). Specific association of Piwi with rasiRNAs derived from retrotransposon and heterochromatic regions in the Drosophila genome. Genes Dev. *20*, 2214–2222.

Sakakibara, K., and Siomi, M.C. (2018). The PIWI-Interacting RNA Molecular Pathway: Insights From Cultured Silkworm Germline Cells. BioEssays *40*, 1700068.

Sato, K., Iwasaki, Y.W., Shibuya, A., Carninci, P., Tsuchizawa, Y., Ishizu, H., Siomi, M.C., and Siomi, H. (2015). Krimper Enforces an Antisense Bias on piRNA Pools by Binding AGO3 in the Drosophila Germline. Mol. Cell *59*, 553–563.

Shibata, N., Kashima, M., Ishiko, T., Nishimura, O., Rouhana, L., Misaki, K., Yonemura, S., Saito, K., Siomi, H., Siomi, M.C., et al. (2016). Inheritance of a Nuclear PIWI from Pluripotent Stem Cells by Somatic Descendants Ensures Differentiation by Silencing Transposons in Planarian. Dev. Cell *37*, 226–237.

Siomi, M.C., Mannen, T., and Siomi, H. (2010). How does the royal family of Tudor rule the PIWI-interacting RNA pathway? Genes Dev. *24*, 636–646.

Vagin, V. V, Sigova, A., Li, C., Seitz, H., Gvozdev, V., and Zamore, P.D. (2006). A distinct small RNA pathway silences selfish genetic elements in the germline. Science *313*, 320–324.

Vagin, V. V, Wohlschlegel, J., Qu, J., Jonsson, Z., Huang, X., Chuma, S., Girard, A., Sachidanandam, R., Hannon, G.J., and Aravin, A.A. (2009). Proteomic analysis of murine Piwi proteins reveals a role for arginine methylation in specifying interaction with Tudor family members. Genes Dev. *23*, 1749–1762.

Wang, J., Saxe, J.P., Tanaka, T., Chuma, S., and Lin, H. (2009). Mili Interacts with Tudor Domain-Containing Protein 1 in Regulating Spermatogenesis. Curr. Biol. *19*, 640–644.

Wieckowski, M.R., Giorgi, C., Lebiedzinska, M., Duszynski, J., and Pinton, P. (2009). Isolation of mitochondria-associated membranes and mitochondria from animal tissues and cells. Nat. Protoc. *4*, 1582–1590.

Wilczynska, A., Minshall, N., Armisen, J., Miska, E.A., and Standart, N. (2009). Two Piwi proteins, Xiwi and Xili, are expressed in the Xenopus female germline. RNA *15*, 337–345.

Xiol, J., Cora, E., Koglgruber, R., Chuma, S., Subramanian, S., Hosokawa, M., Reuter, M., Yang, Z., Berninger, P., Palencia, A., et al. (2012). A Role for Fkbp6 and the Chaperone Machinery in piRNA Amplification and Transposon Silencing. Mol. Cell *47*, 970–979.

Xiol, J., Spinelli, P., Laussmann, M.A., Homolka, D., Yang, Z., Cora, E., Couté, Y., Conn, S., Kadlec, J., Sachidanandam, R., et al. (2014). RNA clamping by Vasa assembles a piRNA amplifier complex on transposon transcripts. Cell *157*, 1698–1711.

Zamparini, A.L., Davis, M.Y., Malone, C.D., Vieira, E., Zavadil, J., Sachidanandam, R., Hannon, G.J., and Lehmann, R. (2011). Vreteno, a gonad-specific protein, is essential for germline development and primary piRNA biogenesis in Drosophila. Development *138*, 4039–4050.

# 6. Acknowledgement

## 6. Acknowledgement

First of all, I would like to thank professor Dr. Mikiko C. Siomi for giving me fantastic environment for my research for six years. Thanks to her, I tried many experiments whatever I wanted and I collaborated with outstanding researchers outside of our lab. Such a great environment stimulates me and blushed up my works. I am grateful to my mentor, Dr. Kazumichi M. Nishida for teaching me many experiments and told me many tips for them. His sophisticated experimental techniques allowed me to perform complicated assays. Dr. Tetsutaro Sumiyoshi and Dr. Yuka W. Iwasaki help me analyze bioinformatic analyses and build programs to elucidate detailed sequential characters. Dr. Takeshi Kawamura and Dr. Tetsuhiko Kodama performed mass spectrum mass spectrometry analysis for phosphorylated serine identification. Dr. Taro Mannen produced anti-Vret monoclonal antibody. Ms. Hiromi Yamada help in the analyses of Papi-Siwi-Zuc complex formation.

This research is supported by the Japan Society for the Promotion of Science and The University of Tokyo Life Innovation Leadaing Graduate School, GPLLI.